Rotation of Aromatic Solutes in Supercritical CO_2: Are Rotation Times Anomalously Slow in the Near Critical Regime?

M. P. Heitz and M. Maroncelli*

Department of Chemistry, The Pennsylvania State University, 152 Davey Lab, University Park, Pennsylvania 16802

Received: March 27, 1997; In Final Form: May 23, 1997[⊗]

Picosecond fluorescence anisotropy decay measurements are used to examine the rotational dynamics of three solutes, 1,3,6,8-tetraphenylpyrene ("TPP"), 9,10-bis(phenylethynyl)anthracene ("PEA"), and *N,N′*-bis-(2,5-di-*tert*-butylphenyl)-3,4,9,10-perylenedicarboximide ("BTBP") in supercritical CO_2 (35 °C = T_c+ 4 °C) and in a variety common liquid solvents. In liquids the rotation times of all three probes show an approximate proportionality to solvent viscosity, in rough agreement with simple hydrodynamic theories. In supercritical CO_2 two of the probes, TPP and BTBP, are found to exhibit rotation times consistent with the extrapolation of the hydrodynamic trends found in liquid solvents. In the case of BTBP, these results disagree with recently published reports of very long rotation times near the critical point [Heitz and Bright *J. Phys. Chem.* **1996**, *100,* 6889]. However, the rotation times of PEA deviate significantly from hydrodynamic predictions based on the viscosity of the supercritical fluid for near critical densities. In this case, it appears that local density augmentation leads to increased rotational friction on the solute compared to what would be expected on the basis of the bulk solvent properties. Using the observed rotation times, an effective density that is 50−100% greater than the bulk density is estimated for reduced densities (ρ/ρ_c) of 0.8−1. Similar estimates of the extent of local density augmentation are also obtained from the behavior of the electronic frequency shifts of this solute.

I. Introduction

As a result of the unique properties of fluids near their critical points, supercritical fluids are becoming ever more popular as alternatives to liquid solvents in a variety of practical applications.[1,2] In most of these applications the utility of supercritical fluids arises from the tunable solvation environment they provide. For popular fluids such as CO_2, relatively modest changes in pressure near room temperature are sufficient to vary the fluid density all the way from gas-like to liquid-like values. Accompanying such density variations are changes in the fluid's static and transport properties (refractive index, dielectric constant, viscosity, etc.) which dramatically alter its ability to solubilize and solvate various species, as well as affect their transport and chemical reaction dynamics.

One of the more interesting features of supercritical fluids is that near the critical point, where this pressure tunabilty is greatest, the local environment of a dissolved solute may be rather different from that of the bulk fluid. It is now well established that solvent molecules tend to "cluster" around a solute such that the local density of solvent molecules in the vicinity of the solute is appreciably higher than the density of the bulk fluid at a given pressure.[1,3−21] This phenomenon, typically referred to as "local density augmentation", also leads to a local enhancement of the various solvent properties mentioned above. As a result, the influence of a supercritical solvent is often considerably greater than expected based on its bulk properties at a given pressure. Clearly a quantitative understanding of this local density augmentation and how it depends on the solute and fluid considered would be helpful when attempting to choose proper conditions for a given application. In addition, this phenomenon provides an opportunity for fundamental studies of solvation in a regime different from that present in normal liquid solvents, a regime wherein attractive interactions would be expected to play a more important role in determining structure. For these reasons a number of workers have examined local density augmentation in supercritical fluids from a variety of perspectives.

Whereas early work in supercritical solvation focused on studies of the equilibrium solvation of simple solutes,[3−21] most current emphasis is on understanding how the unique features of supercritical solvation might influence chemical reactions. There has been vigorous interest from both the practical side, for example, involving the use of supercritical fluids for enzymatic reactions,[22] and polymerization and materials synthesis processes,[23] as well as from a fundamental viewpoint, where interest is in what supercritical fluids can teach us about basic aspects of solvent−reaction coupling. A recent review by Savage et al.[24] provides an excellent overview of much of this work that has appeared over the last decade. Understanding solvent effects on reaction rates in supercritical fluids is a difficult task, due to the simultaneous operation of a number of solvent-related effects that may be difficult to separate.[25] For example, potential energy surfaces are in general density dependent, and the precise form of this dependence will depend very much on the local density augmentation present in a given system. Since changes in reactive barriers produce exponential changes in reaction rates, it is often difficult to disentangle static and dynamic effects which might be simultaneously operating in a given reaction. For this reason, even in favorable cases interpretations are still often unclear. As an example, we cite the diffusion-limited excimer formation of pyrene, which has been studied independently by three groups.[14,26−28] Each of these groups has drawn different and conflicting conclusions as to whether (and how) this very simple reaction is affected by local density/concentration augmentation.

While a great deal is currently being learned about supercritical fluids as reaction media through direct studies of reaction rates, the aforementioned difficulties make it clear that studies

[⊗] Abstract published in *Advance ACS Abstracts,* August 1, 1997.

S1089-5639(97)01096-7 CCC: $14.00

of simpler, nonreactive dynamics are also of value. In particular, studies of how the dynamics of isolated solutes respond to changes in fluid conditions should provide useful insights into the likely behavior of more complex, reactive systems. However, to date surprisingly little information is available on the nonreactive dynamics of solutes in supercritical fluids. Of most direct relevance to bimolecular reaction kinetics would be measurements of translational diffusion. Unfortunately, the techniques commonly used to study tracer diffusion in liquid solvents are difficult to apply in the supercritical regime, and reliable data, especially in the most interesting regime below the critical density, are virtually nonexistent.[29] Studies of vibrational and rotational relaxation can also provide insight into the nature of frictional effects in supercritical solvents. Thus far, only a few studies of vibrational relaxation have focused on the near critical regime.[30−33] Two recent studies that can be readily compared to the work undertaken here are the studies of Pan and MacPhail[32] and Fayer and co-workers.[33] In the first of these, Pan and MacPhail employed a Langevin equation analysis of the Raman band shapes of the C−H stretch in cyclopentane-d_9 to estimate the friction on the pseudorotation coordinate as a function of density in supercritical CO_2 ($T_r \equiv T/T_c = 1.06$).[32] They observed deviations from the density dependence expected based on an Enskog model for the friction and attributed these deviations to the presence of local density augmentation, which they found could be reasonably estimated from the bulk solvent compressibility. Their results can be interpreted as indicating a maximal "frictional" density augmentation of ∼40% at $\rho_r \equiv \rho/\rho_c \approx 0.8$. In a picosecond time-resolved infrared study, Fayer and co-workers[33] measured both the vibrational frequency and lifetime of the asymmetric stretching mode of $W(CO)_6$ in near critical CO_2. At a temperature of 2 °C above critical ($T_r = 1.006$) these authors noted that both the frequency and lifetime remained nearly constant for a factor of 2 change in density near ρ_c. This density invariance was largely eliminated by moving away from the critical temperature by as little as 20 °C. From their data one can estimate a maximal effective density augmentation of ∼60% for $\rho_r \approx 0.7$ at the lower temperature studied. A noteworthy aspect of this latter work is that nearly identical estimates for the local density augmentation are obtained from both the vibrational frequencies and lifetimes.

Several groups have also begun to investigate the rotational dynamics of isolated solutes in supercritical fluids.[34−39] Howdle and Bagratashvili[36] measured the rotational Raman spectrum of H_2 in CO_2 (in an 18 mol % mixture). They observed that the widths of the S-branch transitions of H_2, which monitor the friction on rotational motion, show a broad density-independent region, similar to the behavior observed in the $W(CO)_6$ study. It is surprising to observe such large effects in what might be expected to be a repulsive mixture,[40] and it would be interesting to see if this behavior persists in a more dilute mixture.

Three other studies, closely related to the work undertaken here, have utilized emission anisotropies to measure the (excited-state) rotation times of fluorescent solutes. In the earliest of these, Bright and co-workers[37] measured the rotation times of the solvatochromic probe "PRODAN" [6-propionyl-2-(dimethylamine)naphthalene] in supercritical N_2O using a combination of steady-state anisotropy and fluorescence lifetime measurements. On the basis of emission frequency shifts, they reported a 250% enhancement (i.e., $\rho_{local} = 3.5\rho_{bulk}$) in the local density of PRODAN near the critical density ($T_r = 1.01$), which they noted is much larger than values observed in other systems. Even more interesting behavior was found for the rotation times of this probe. Bright and co-workers reported that the rotation times of PRODAN increase from a nearly constant value of ∼10 ps at high N_2O densities to ∼40 ps just below the critical density. This observation implies that near the critical point of N_2O, where bulk viscosities are an order of magnitude smaller, rotation of PRODAN is comparable to or slower than that in typical liquid solvents.[41] Even given the effects of local density augmentation, this behavior is unexpected. However, a very recent study by Heitz and Bright showed that apparently similar effects were present in a completely different system, "BTBP" (see Figure 1) in both supercritical CO_2 and CF_3H ($T_r = 1.01$).[38] They observed that the rotation times of BTBP were roughly in accord with hydrodynamic expectations at high densities ($\tau_{rot} \approx 40$ ps). But, as with the previous study, decreasing the density in either supercritical solvent led to an *increase* in the rotation time of this solute. In CO_2 the largest rotation time was observed to be ∼180 ps at $\rho_r = 1.4$ (the lower limit of their data), and in CF_3H it was ∼300 ps near $\rho_r = 1$. Thus, decreasing the bulk density of the supercritical fluid apparently leads to a nearly 8-fold increase in rotation time as the critical density is approached.

In contrast to these two examples, the recent results of Anderton and Kauffman[39] point to much less dramatic effects of supercritical fluid density on rotation. Anderton and Kauffman measured rotation times of diphenylbutadiene (DPB) and 4-hydroxymethylstilbene (HMS) in supercritical CO_2 ($T_r = 1.01$). With both solutes they found what would be considered more "normal" behavior, namely, that rotation times decreased upon isothermally decreasing the bulk solvent density. Between high density ($\rho_r \approx 2$) and near critical densities they found that the DPB rotation time decreased by about 50% (6 to 4 ps), whereas that of HMS decreased nearly 3-fold (11 to 3 ps). Anderton and Kauffman modeled the observed density dependence in terms of a free-space model for rotational dynamics[42] and came to the conclusion that there is little or no effect of local density augmentation on the rotation of DPB, and there is only a modest 30−40% enhancement in the case of HMS.[39]

Thus, the available results concerning rotational motion of solutes in supercritical fluids paint a somewhat confusing picture of how supercritical solvation might affect simple nonreactive dynamics. The anomalously slow rotation times observed by Bright and co-workers[37,38] are difficult to rationalize. However, the fact that similar results are seen for several solute/solvent combinations leads one to think that it might be a general phenomenon. If so, then why is this behavior apparently absent in the cases of DPB and HMS?

The present work was largely motivated by the desire to answer these questions. We have used the time-resolved fluorescence anisotropy technique to study the rotational dynamics of three solute molecules in supercritical CO_2. The solutes examined here are 1,3,6,8-tetraphenylpyrene (TPP), 9,10-bis(phenylethynyl)anthracene (PEA), and *N*,*N*′-bis(2,5-di-*tert*-butylphenyl)-3,4,9,10-perylenedicarboximide (BTBP). The chemical structures and space-filling representations of these solutes are provided in Figure 1. These particular solutes were chosen mainly for their large size, which enables us to accurately measure anisotropy decay times using the time-correlated single-photon-counting (TCSPC) method. BTBP was specifically chosen in order to confirm the behavior observed previously using frequency-domain fluorimetry. In addition, BTBP has been extensively used as a rotation probe in liquid solvents by Ben-Amotz and co-workers.[43] PEA has also been recently used in a study of bimolecular quenching in supercritical fluids.[44] However, to our knowledge the rotational dynamics of neither PEA nor TPP has been studied previously, even in simple liquid solvents. Thus, in order to calibrate the "normal" hydrodynamic

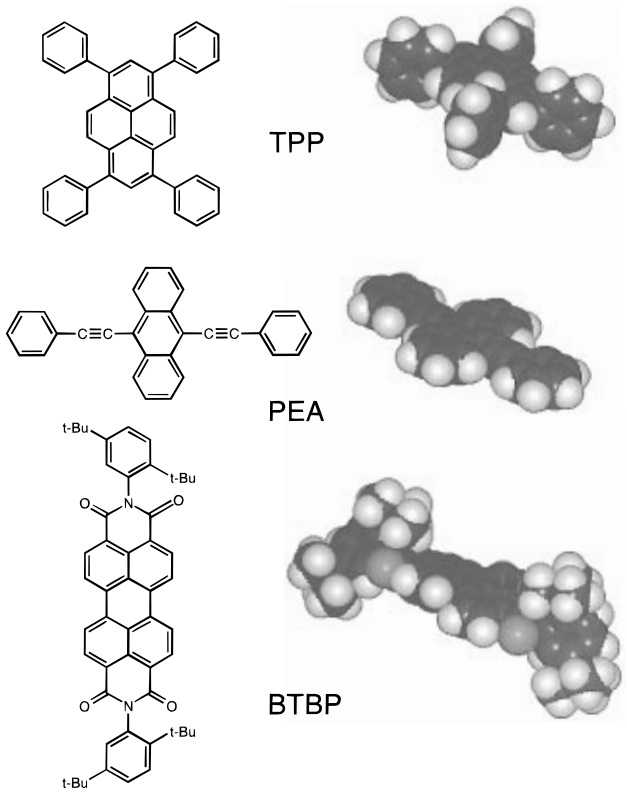

Figure 1. Molecular structures and space-filling representations of TPP, PEA, and BTBP. The geometries depicted by the space-filling representations are created from the energy-minimized configurations. See text, section III-A.

behavior of these probes we also report here the results of rotational measurements for these molecules in a wide variety of room temperature liquid solvents.

The structure of the remainder of this paper is as follows. In section II, we describe experimental details related to the preparation of supercritical samples and their measurement. Section III discusses the predictions of hydrodynamic theory for the systems studied and discusses the two methods used to determine rotation times. The main results of this study are then presented in section IV. In part IV-A we first use the electronic spectral shifts of the solutes to provide one means for assessing the extent of local density augmentation. We then go on in part IV-B to consider the solute rotational dynamics, making extensive use of the liquid solvent data to calibrate our expectations in the supercritical fluid. The results obtained here directly contradict the previous results obtained with BTBP in that we do not observe its rotation times to be anomalously slow or to decrease with decreasing density. Rather, the rotation times of BTBP and the other two solutes reflect only behavior that would be expected from the sorts of local density augmentation reported in most solvatochromic studies. In the case of PEA, the most soluble of the three probes, we find that both the spectral shifts and the rotation times provide a consistent view of the local density augmentation in CO_2, which amounts to ~100% augmentation at $\rho_r = 0.8$. Finally, in section V we summarize our results in comparison to prior work and briefly address the possible sources of the difference between the present results with BTBP and those of Heitz and Bright.[38]

II. Materials and Experimental Techniques

The probe molecules used here were obtained from several sources. *N*,*N*′-Bis(2,5-di-*tert*-butylphenyl)-3,4,9,10-perylenedicarboximide (BTBP) and 9,10-bis(phenylethynyl)anthracene (PEA) were from Aldrich, and 1,3,6,8-tetraphenylpyrene (TPP) was from Chem Service, West Chester, PA. All probe molecules were used as received. Liquid solvents (Aldrich) were either HPLC or spectral grade and were used without further purification. Carbon dioxide (<10 ppm O_2) was purchased from MG Industries and was purified by passing through an oxygen trap prior to entering the supercritical apparatus.

Samples for the liquid studies were prepared by adding an aliquot of a stock solution to a standard 1 cm fluorescence cuvette and evaporating the solvent using a gentle stream of N_2. The resulting concentration of the solutions was always $<5 \times 10^{-6}$ M. At these concentrations, the optical density (OD) was <0.1 at the wavelength of maximum absorbance. All steady-state and time-resolved measurements in liquids were performed at room temperature, 295 ± 1 K.

For measurements in supercritical CO_2, we used a 2 cm path length high-pressure cell fabricated from stainless steel. Quartz windows sealed with Teflon O-rings provided three-way optical access to the cell in a T-format geometry. To prepare a sample for supercritical fluid investigations, the probe molecule was added to the high-pressure cell in the same manner as for liquid samples, again such that the concentration was $<5 \times 10^{-6}$ M. The cell was flushed with CO_2 to remove any residual solvent or oxygen and then sealed and heated to the desired temperature using a thermostated water circulator. Fluid from a syringe pump (Isco, Model 100-DM) was introduced into the cell, adjusted to the desired starting pressure, and allowed to equilibrate. Homogeneity of the solution was ensured by using a magnetically coupled stir bar. Temperature and pressure were measured by a standard thermocouple and digital pressure gauge with accuracies of ±0.3 K and ± 20 psi, respectively.

We report experimental parameters for CO_2 in reduced units using the critical constants $P_c = 1071$ psia, $T_c = 304.2$ K, and $\rho_c = 0.468$ g/cm^3.[45] In these experiments the temperature was 308 K, T_r ($\equiv T/T_c$) = 1.01, maintained to ±0.2 K. The pressure range accessed was from 1100 to 3500 psia, which was held constant to within ±1 psia. Densities corresponding to a given *P*,*T* combination were calculated using a modified Benedict−Rubin−Webb equation of state,[46] and viscosities were calculated using the method of Vesovic et al.[47,48] Values of the refractive index at a given density were calculated from the modified Lorentz−Lorenz relationship of Besserer and Robinson.[49] Corresponding to the pressure range noted above, the reduced density ($\rho_r \equiv \rho/\rho_c$), viscosity, and refractive index studied here cover the ranges 0.6−1.9, 0.02−0.09 cP, and 1.06−1.21, respectively.

Steady-state absorption and emission spectra were recorded on a Perkin-Elmer Lambda 6 UV−vis spectrophotometer and a Photon Technology International QuantaMaster fluorometer, respectively. The instrumental parameters were chosen to provide resolutions of ~1 nm in absorbance and ~2 nm in emission. All spectra were blank subtracted, and fluorescence spectra were corrected for instrumental response.

Time-resolved fluorescence decays were measured using the time-correlated single-photon-counting (TCSPC) technique. The excitation source consisted of a picosecond Ti:sapphire laser (Coherent, Model 900) pumped by a CW, multiline argon ion laser (Coherent Innova 415). Output pulses had a width of ~2 ps (fwhm of autocorrelation) at a repetition rate of 76 MHz. The mode-locked output of the Ti:sapphire was directed into a pulse picker (Coherent 9200) where the repetition rate was reduced to 4 MHz prior to frequency doubling in a CSK Model 8312 harmonic generation assembly. Emission from the sample was spectrally resolved using a 0.1 m subtractive double monochromator (American Holographics, DB-10) prior to

TABLE 1: Summary of Probe Parameters

		hydrodynamic parameters (295 K)					inertial parameters	
probe[a]	volume (Å^3)	*a* (Å)	*b* (Å)	*c* (Å)	τ_{stick}[b] (ps/cP)	τ_{slip}[b] (ps/cP)	I_{eff}[c] 10^3(amu Å^2)	τ_{eff}[c] (ps)
TPP	464	1.73	8.00	8.00	257	43	4.6	3.0
PEA	360	1.70	4.77	10.60	300	122	4.5	3.0
BTBP	720	3.29	4.00	13.06	518	280	18.3	6.0
PRODAN	235	1.70	4.43	7.43	133	35	0.6	1.0
DPB	206	1.70	3.54	8.17	141	59	1.8	1.9
HMS	209	1.70	3.77	7.79	132	48	1.6	1.8

[a] For reference we also list parameters for several of the probe solutes that have been employed in prior studies of rotation in supercritical fluids. [b] The calculated stick and slip anisotropy decay functions are not always exact single-exponential decay functions. In the case of nonexponential behavior the times reported are weighted averages as in eq 3. [c] $I_{eff} = ((1/I_{aa}) + (1/I_{bb}))^{-1}$ for transition moment along *c*, and $\tau_{eff} = (2\pi/9)(\sqrt{I_{eff}/k_bT})$.

detection with a 6 μm microchannel plate photomultiplier (Hamamatsu, R3809 U). The MCP-PMT signal was amplified (Phillips 6954 amplifier), conditioned by a modified constant-fraction discriminator (CFD, Tennelec TC 454), and used as the start pulse for the biased time-to-amplitude converter (TAC, Tennelec TC 864). The stop pulse for the TAC was generated by directing a portion of the excitation pulse to a fast photodiode (Opto-Electronics PD-30), the output of which was also conditioned by the CFD. Finally, the TAC output was recorded on a computer-based multichannel analyzer (PCA3, Oxford Instruments). The overall instrument response of this system, determined using a scattering solution, was typically 25−30 ps fwhm. A single anisotropy measurement consisted of collecting emission decays polarized parallel (||) and perpendicular (⊥) and at the "magic" angle (54.7°).

Excitation for BTBP and PEA was at 450 nm, whereas TPP was excited at 385 nm. Fluorescence was monitored at 540, 500, and 440 nm for BTBP, PEA, and TPP, respectively. Emission was collected using bandwidths of 2 nm for decays in liquid solvents and 20 nm in supercritical CO_2. The time-resolved fluorescence data are collected over a 8 ns time window (2048 channels) using a bin size of 4.1 ps per channel.

III. Methods of Data Analysis

A. Hydrodynamic Modeling. Hydrodynamic models provide useful semiquantitative descriptions of the rotational dynamics of large solutes in normal liquid solvents.[50] Such models result in rotation times (τ_{rot}) being expressed in terms of the modified Stokes−Debye−Einstein (SED) equation:

$$\tau_{rot} = \frac{\eta V_p}{k_B T} fC \qquad (1)$$

where η is the fluid viscosity, V_p the volume of the probe solute, and k_BT is Boltzmann's constant times the absolute temperature. The factor *f* in eq 1 accounts for the shape of the solute, and *C* allows for possible variation of the hydrodynamic boundary conditions. For a spherical body, which was the shape considered in the original SED formulation, rotational motion is isotropic and *f* and *C* are both unity for stick boundary conditions. The situation is more complex for molecules that are not spherical in shape. First, the rotational motion may be anisotropic, in which case a complete description may require the use of a second-rank tensor rather than a single diffusion constant or time. (Anisotropic diffusion may give rise to five distinct time constants in the decay of second-rank rotational correlation functions of the sort studied here.[50,51]) Fortunately, the shapes of many molecules are such that effectively isotropic rotation is observed in most experiments. A second complication is that while the proportionality between τ_{rot} and $\eta V_p/k_BT$ is still valid for a nonspherical body, calculation of the *f* and *C* factors is not trivial for molecules of arbitrary shape. For this reason, virtually all applications of the hydrodynamic formalism assume that molecules may be represented as ellipsoidal bodies. Analytic expressions for *f* have been derived for such shapes in the case of stick boundary conditions.[52] In the case of slip boundary conditions one also has the additional correction factor *C* ($C < 1$), which has been determined numerically and can be found in tabulated form.[53]

In the present work, we compare experimentally observed rotation times to the predictions of hydrodynamic calculations assuming an ellipsoidal shape. We define an effective ellipsoid in the following manner. The probe's molecular geometry is determined from a semiempirical AM1 calculation[54] and its volume calculated using van der Waals increments.[55] From the optimized structure, semiaxes for the ellipsoidal representations are estimated which preserve the van der Waals volume of the molecule. One axis is defined as the longest dimension of the probe molecule, and the other two axes are chosen such that a visual "best fit" is obtained. PEA and BTBP are best represented by an asymmetric near prolate shape, and TPP by an oblate shape. Of course, there is considerable latitude in defining the best ellipsoidal shape for these molecules, since, as Figure 1 reveals, none of them closely resemble ellipsoidal bodies. For example, the geometry of TPP is such that the four phenyl rings are oriented orthogonally to the pyrene moiety. To describe TPP as an oblate symmetric top clearly misses its "paddle wheel" shape. Similar problems arise with the other probes. Nonetheless, given the "best" choice of ellipsoidal shape, the diffusion constants for stick and slip limits are calculated.[51−53] In all cases we assume the absorption and emission transition moments are parallel. The analysis of the experimental data confirms the validity of this assumption. For the near prolate molecules PEA and BTBP, we take the direction of these moments to be that of the long molecular axis, while for TPP they are assumed to lie somewhere within the pyrene plane. The collection of volumes and axial dimensions (*a*,*b*,*c*) for TPP, PEA, and BTBP as well as the stick and slip rotation times that result are listed in Table 1. As we will show shortly, in spite of the difficulties with ellipsoidal representations, the stick hydrodynamic predictions still yield reasonable estimates of the observed rotation times.

B. Experimental Determination of *r(t).* Rotation times were determined from time-resolved fluorescence data using two different methods: iterative reconvolution fitting and an integral approach that involves the difference between parallel and perpendicular emission decays. Iterative reconvolution fitting is the standard method for determining time constants from a single fluorescence decay or from anisotropy decay data, and the details of reconvolution algorithms can be found

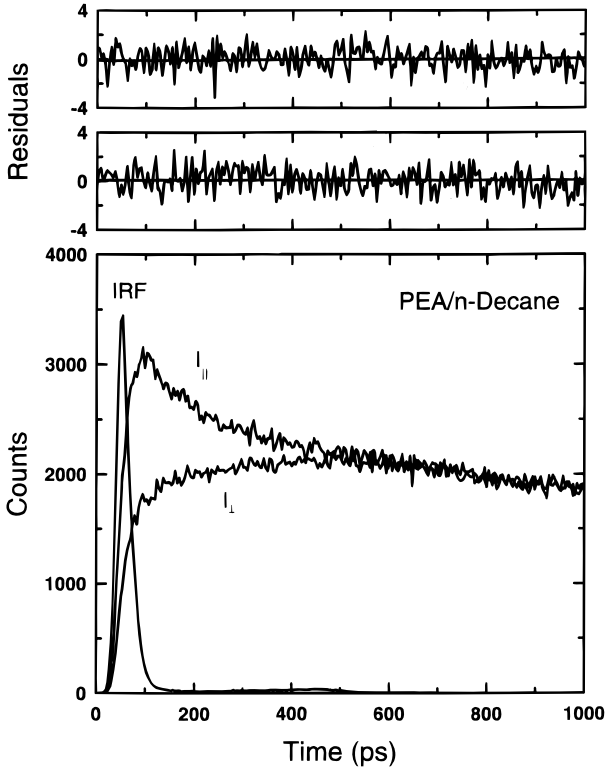

Figure 2. Representative polarized emission decays and anisotropy fits of PEA in liquid *n*-decane at 295 K. The bottom panel shows the instrument response function (IRF) and the polarized intensity decays parallel ($I_{||}$) and perpendicular ($I_{\perp}$) to the exciting radiation. The two upper panels are the residuals of the parallel (top) and perpendicular (bottom) components resulting from the iterative reconvolution fit of the time-resolved data.

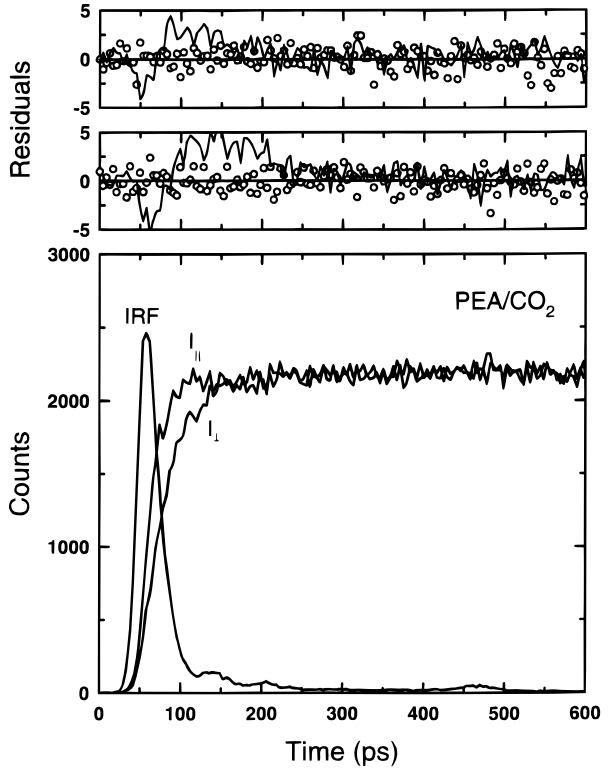

Figure 3. Representative polarized emission decays and anisotropy fits of PEA in supercritical CO_2 at 1300 psia ($\rho_r \approx 1.4$) and 308 K ($T_r = 1.01$). The bottom panel shows a typical instrument response function (IRF) in the high-pressure cell using PEA/CO_2 as the scattering solution along with the polarized intensity decays parallel ($I_{||}$) and perpendicular ($I_{\perp}$) to the exciting radiation. The two upper panels are the residuals of the fits to the parallel (top) and perpendicular (bottom) components. The lines show the residuals of a fit in which the magic angle and polarized emission decays are both modeled by a single-exponential decay law. The open circles show the residuals when a biexponential decay law is used for the magic angle decay while retaining a monoexponential decay law for the polarized emission decays. See section III-B for a more complete description.

elsewhere.[50,56] The integral approach is an alternative method we have devised for determining rotation times in supercritical fluids; it is described fully in the Appendix of this paper. Here we discuss both methods only briefly, stressing the special features relevant to anisotropy studies in supercritical fluids.

In iterative reconvolution fitting one assumes that the population *(m(t))* and anisotropy *(r(t))* decays can be expressed by multiexponential functions of time:

$$m(t) = m(0)\sum_i a_i \exp(-t/\tau_i) \tag{2}$$

and

$$r(t) = r(0)\sum_i b_i \exp(-t/\tau_{\mathrm{rot},i}) \tag{3}$$

with $\sum a_i = \sum b_i = 1$. These functions are directly related to the "ideal" emission decays collected with parallel ($i_{||}(t)$), perpendicular ($i_{\perp}(t)$), and magic angle ($i_m(t)$) polarizations via the relations

$$m(t) = \frac{1}{3}\{i_{||}(t) + 2i_{\perp}(t)\} = i_m(t) \tag{4}$$

and

$$r(t) = \frac{I_{||}(t) - I_{\perp}(t)}{I_{||}(t) + 2I_{\perp}(t)} \tag{5}$$

These ideal decays differ from the observed emission decays due to (1) the possible presence of a nonzero background, (2) differential polarization sensitivity of the detection apparatus, and (3) temporal broadening caused by a finite instrumental response function (IRF). The latter is the decay profile that would be observed from the instrument given a sample with a delta function emission response. A nonlinear least-squares algorithm[57] is used to determine the values of the multiexponential parameters and relative normalization factors that provide the best simultaneous fit to the observed set of parallel, perpendicular, and magic angle decays.

Representative decays and their reconvolution fits are shown in Figures 2 and 3. Figure 2 displays data for PEA in *n*-decane, collected with a sample in a standard fluorescence cuvette. The bottom panel shows the parallel and perpendicular emission decays along with the instrument response. The instrument function for this data was recorded using a scattering solution of dilute nondairy creamer in water. The top two panels show the residuals of fits to these data using a model in which both *m(t)* and *r(t)* are monoexponential functions of time. The randomness of the residuals indicates the overall goodness of fit. Although we do not show the magic angle decay here, either simultaneous or independent fitting of these data lead to the same *m(t)* decay law and the same quality of fit ($\chi_\nu^2 = 1.05$) as illustrated here. For all solute/solvent combinations the data could be well represented by a monoexponential *m(t)* function and in most cases (see section IV-B) a monoexponential *r(t)* function as well.

In contrast to the data collected in liquid solutions, experimental data acquired in the SCF cell were less readily fit (Figure 3). Collection of an instrument response function using a scattering solution in the supercritical cell proved to be impractical since the cell must be depressurized, broken down, and cleaned in order to prepare a solution. Therefore, to obtain an IRF for the supercritical experiments, we employed the Rayleigh scattering present in a low-density sample of the CO_2 solution itself. Since only minute quantities of the probes were dissolved at the lowest density (almost undetectable by steady-state fluorescence), there was no interference from fluorescence at the Rayleigh wavelength. Use of Rayleigh scattering for an IRF worked as well as using a separate scattering solution when tested in liquid (cuvette) samples. Unfortunately, this practice never led to the same quality of fits in supercritical samples. The difficulty is illustrated in Figure 3, which presents data collected with PEA in CO_2 (1300 psia, $\rho_r = 1.4$). The top two panels of this figure show two sets of residuals each. The solid curves are the residuals from the fit to a model in which both *m(t)* and *r(t)* are monoexponential functions. Neither the polarized component nor the magic angle decay (not shown) is well fit by a monoexponential model ($\chi_\nu^2 = 1.5$). To adequately fit the data, a second exponential term must be added to the *m(t)* decay law (keeping *r(t)* a monoexponential function). In the case at hand, addition of a 25%, 10 ps component is required in order to achieve the fit shown by the open symbols in Figure 3. These data are typical of what we observe in most supercritical fluid samples. In all instances a small fraction (usually $\leq$25%) of a fast time constant ($<$30 ps) in *m(t)* was needed to achieve good fits to the data. While it is clear that such components are due to scattering within the supercritical fluid cell, we were unable to eliminate them completely from the data. (Similar fitting artifacts are observed in cuvette samples if absorbing glass is not used to prevent the excitation beam from hitting the exit face of the cuvette.) The cell was fitted with a piece of absorbing glass that acted as a beam stop, but evidently the small amount of scattered light that is not eliminated in this way is responsible for the artifact. All of the supercritical data were therefore fit to a biexponential *m(t)* model in order to extract *r(t)* information. We note that the long component of *m(t)*, which reflects the true lifetime decay, is unaffected by the presence of this additional component. Most importantly, the anisotropy decays do not appear to be significantly affected by use of the biexponential *m(t)* fits. This conclusion is based on comparisons between liquid samples in cuvettes and in the supercritical fluid cell.

In light of the above difficulties in obtaining an IRF that yields accurate reconvolution fits, we also employed an alternative approach for determining rotation times from the emission decays in supercritical fluid samples. This method, which we will call the "integration method", relies on the fact that the rotation time is related to *r(0)* and the integral under the suitably tail-matched intensity difference curve, $I_{\parallel}(t) - I_{\perp}(t)$. Although the method also uses an IRF, its results are relatively insensitive to the detailed shape of the IRF. Figure 4 illustrates the analysis of the two PEA data sets from Figures 2 and 3 using this integral approach. The decaying trace on each panel is the observed *r(t)* function (not deconvoluted from the instrumental response), while the rising curve is its integral, from which the average rotation time is derived. In addition to being less affected by the IRF, plots such as those shown in Figure 4 provide visual estimates of the uncertainties in the measured rotation times. The data shown here are typical. Whereas the liquid samples afforded rotation times with a precision on the order of 5%, the supercritical samples, due to their lower signal levels and faster

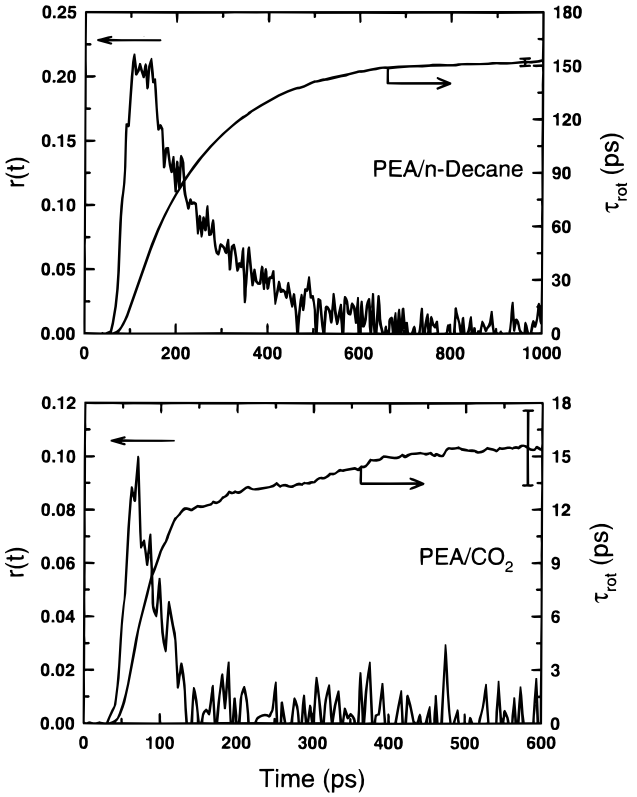

Figure 4. Examples of anisotropy decays in liquid and supercritical CO_2 illustrating the integral method of analysis. The data presented in the upper and lower panels correspond to the same data sets used in Figures 2 and 3, respectively. The noisier curve in each plot (left axis) is the anisotropy decay curve, ($r(t)$), that is obtained without deconvolution of the instrumental response function. The smoother curve (right axis) is the weighted integral over the $r(t)$ data, which provides the estimate of the rotation time, τ_{rot}. The error bars in each panel show the typical estimated uncertainty for this method of analysis. Details related to these calculations are given in the Appendix.

rotation times, yielded an uncertainty of $\sim$15$-$20%. Similar estimates of uncertainties in rotation times are also derived from the reconvolution fitting.

It is reassuring that these two methods yield results that are mutually consistent to within $\pm$9% for liquid samples and $\pm$15% for supercritical samples. Since both methods appear to produce equally reliable results, the values for rotation times in supercritical fluids reported here are averages of the numbers obtained by the two methods. In addition, all anisotropy decay measurements were taken twice, using two independently prepared solutions and the same series of pressures. The results from these independent data sets were averaged in order to produce the final results reported in Table 4.

Finally, we comment on the likely accuracy of our measured rotation times in supercritical solvents. Even for the large solutes chosen for the present study, the rotation times observed in supercritical CO_2 are comparable to the temporal width of our instrumental response. To examine whether our instrumentation should be expected to provide accurate results under these conditions, we measured rotation times for the smaller solute coumarin 153 (C153) in several liquids using the present TCSPC instrument and compared them to measurements recently made with much higher time resolution (0.1 ps) using the fluorescence upconversion technique.[58] The results of this comparison are provided in Table 2. The rotation times measured with the present methods are within 10% of those measured with much higher time resolution and indicate that our TCSPC measurements of rotation times be should be reliable down to times on the order of 10 ps.

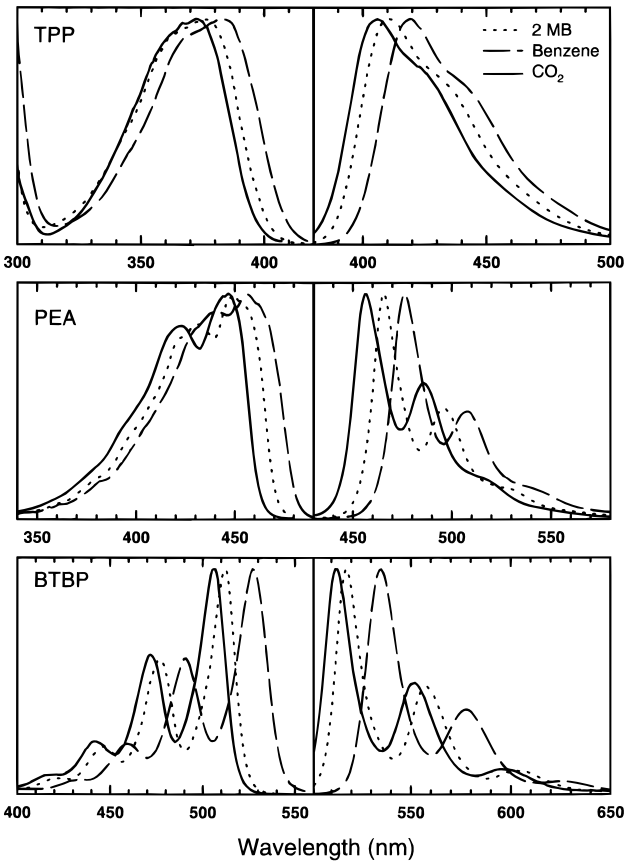

Figure 5. Representative steady-state excitation (left) and emission (right) spectra of TPP, PEA, and BTBP in various solvents. Specific examples are shown for each probe in 2-methylbutane (2-MB; ···), benzene (- - -), and supercritical CO_2 (—). The spectra in supercritical CO_2 correspond to $\rho_r \approx 1.9$ and $T_r = 1.01$.

IV. Results and Discussion

A. Steady-State Spectroscopy and Emission Lifetimes. Before discussing rotational dynamics it is useful to consider the steady-state spectra of the various probes for what they reveal about solvation in supercritical CO_2. Figure 5 shows a set of representative excitation and emission spectra of all three probes in the liquid solvents 2-methylbutane and benzene and in supercritical CO_2 ($\rho_r = 1.9$). The spectra exhibit some vibronic structure, which is slightly more evident in emission than in excitation. Both the excitation and emission spectra shift to the red as the polarizability of the solvent increases from CO_2, to 2-methylbutane, to benzene. Except for a slight broadening, there is little change in the shape of the spectra with solvent. In addition, the shifts in excitation and emission are comparable in all cases such that there is little change in the Stokes shift with solvent.[59] Similar observations can be made about the spectra in supercritical CO_2 as a function of density. One such set of data (PEA at 35 °C) is shown in Figure 6. Apart from the exponential decrease in emission intensity at lower density (inset), which reflects the decreasing solubility in the rarefied fluid, there is little to distinguish these spectra from the spectra in typical liquid solvents. We note that the spectra at low densities show no signs of possible solute−solute interactions or the presence of crystalline aggregates, which might possibly complicate the interpretation of the emission data.[60]

TABLE 2: Comparison of C153 Rotation Times (295 K) Measured by Time-Correlated Single-Photon Counting and Fluorescence Upconversion

	rotation time (ps)		
solvent	TCSPC−reconvolution	TCSPC−integral	fluorescence upconversion[a]
n-hexane	14	16	14
acetone	19	21	19
DMF	48	52	47
formamide	193	187	185

[a] Fluorescence upconversion measurements from this laboratory.[58]

In order to examine the solvent dependence of the spectra more quantitatively, we compare the observed shifts to the predictions of continuum models of solvatochromism.[10] For nondipolar solutes of the sort studied here, such models predict that transition frequencies should vary with dielectric properties of the solvent as

$$\nu(\text{solution}) = \nu(\text{vapor}) + A\left(\frac{n_D^2 - 1}{2n_D^2 + 1}\right) + B\left(\frac{\epsilon_0 - 1}{\epsilon_0 + 1}\right) \quad (6)$$

where n_D and ϵ_0 are the optical index of refraction and static

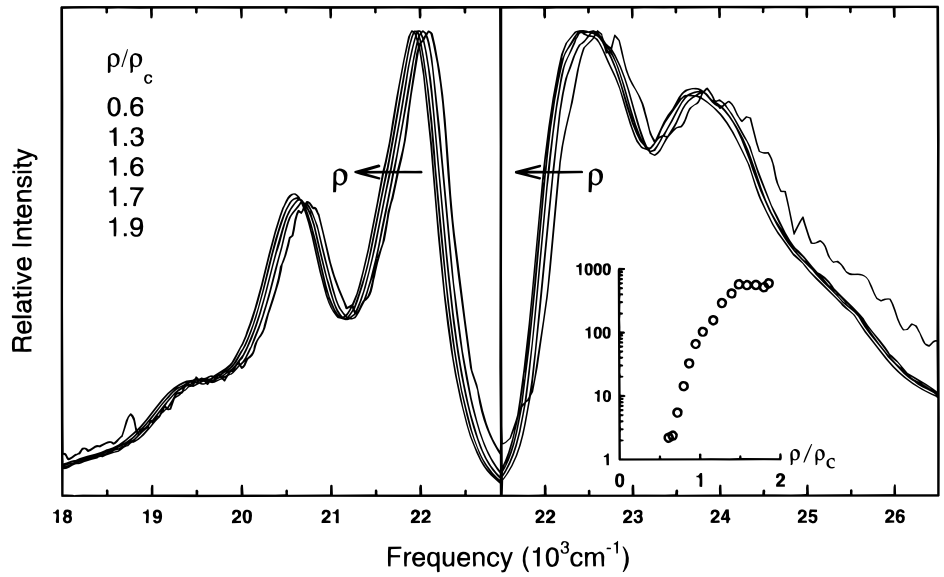

Figure 6. Steady-state emission (left) and excitation (right) spectra of PEA in supercritical CO_2 shown as a function of density (ρ). The values of reduced density (ρ/ρ_c) are 0.6, 1.3, 1.6, 1.7, and 1.9. The arrows indicate the direction of increasing density. The inset shows the increase in relative emission intensity as a function of reduced density resulting from the density-dependent solubility of PEA in supercritical CO_2.

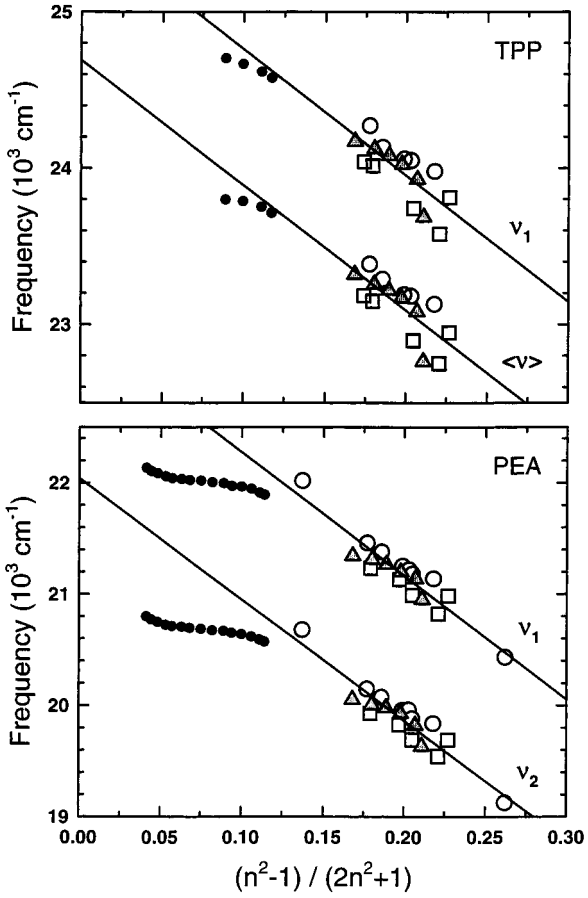

Figure 7. Steady-state emission frequency shifts for TPP and PEA in liquid solvents (large symbols) and supercritical CO_2 (small filled circles) versus the reaction field factor of eq 7. The large symbols represent solvent classes as follows: nonpolar (○), polar aprotic (□), and polar protic (alcohols, ▲). The supercritical data shown is at $T_r = 1.01$ for both TPP and PEA. Two characteristic frequencies of the spectrum are shown in each case. For TPP ν_1 denotes the position of highest intensity (cf. top panel of Figure 5), whereas $\langle\nu\rangle$ is the average frequency (first moment) of the emission spectrum. In the case of PEA, the well-resolved vibronic structure is used with ν_1 and ν_2 corresponding to the peak frequencies of the two most intense vibronic features (cf. middle panel of Figure 5). The solid lines in both panels are the linear regressions to all of the liquid state values. Similar results were observed for BTBP (not shown).

dielectric constant of the solvent and *A* and *B* represent the coupling between the solvent and solute due to dispersion interactions (*A*) and solvent dipole, solute-induced dipole interactions (*B*).[61]

In Figure 7 we illustrate the magnitudes of shifts observed in liquid solvents and supercritical CO_2 by plotting the emission frequencies of TPP and PEA as a function of the reaction field factor,

$$f_1(n_D^2) \equiv \frac{n_D^2 - 1}{2n_D^2 + 1} \tag{7}$$

This factor, which appears in the *A* term in eq 6, is a measure of the electronic polarizability of the solvent, which determines how strong its dispersion interactions with the solute will be. Consider first the liquid solvents, shown with the larger symbols ($f_1(n_D^2) > 0.13$). Figure 7 reveals that there is a reasonable correlation between the observed emission frequencies in a variety of liquid solvents and $f_1(n_D^2)$, indicating that dispersion interactions are primarily responsible for the spectral shifts observed in these solutes. (Similar quality correlations are observed for excitation frequencies and in the cases of BTBP, not illustrated here.) However, there are also systematic differences observed with different solvent types. Here and in the following figures we distinguish three classes of liquid solvents: nonpolar solvents (open circles), polar aprotic solvents (squares), and hydrogen bond donating solvents (triangles). The source of the deviation from the average correlation with $f_1(n_D^2)$ shown by the solid lines is due to what has been called the "solvent Stark effect", which is modeled by the *B* term in eq 6.[61,62] Thus, the scatter illustrated in Figure 7 is considerably reduced when these data are fit to multiple regressions including both terms in eq 6. For example, the ν_1("0−0") emission frequencies in Figure 7 are best fit by the relations

$$\nu_1(\text{TPP}) = 26.009 - 9.267 f_1(n_D^2) - 0.322 f_2(\epsilon_0) \qquad (N = 16, R = 0.933)$$

and

$$\nu_1(\text{PEA}) = 23.574 - 11.26 f_1(n_D^2) - 0.277 f_2(\epsilon_0) \qquad (N = 19, R = 0.982)$$

where $f_2(\epsilon_0)$ denotes the final term in eq 6, and *N* and *R* are the number of data points and the regression coefficient of the fit. (The regressions of the data that neglect the $f_2(\epsilon_0)$ term have correlation coefficients of 0.766 (TPP) and 0.940 (PEA).) Taking into account the roughly 4-fold greater range of $f_2(\epsilon_0)$ than $f_1(n_D^2)$, the ratio of the *A* and *B* coefficients indicates that the solvent-dipole-induced interactions represented by $f_2(\epsilon_0)$ are only 10−15% of the overall shift. Thus, as already noted, the dominant contribution to these shifts, and probably also to the solvation energies of these solutes, comes from dispersion interactions with the solvent.

The data in Figure 7 shows that the shifts observed in supercritical CO_2 at 35 °C (small filled circles) do not fall cleanly on the correlations with $f_1(n_D^2)$ established by the liquid solvents. Although the deviations of the highest density CO_2 results (largest values of $f_1(n_D^2)$) from the regression lines are no more than the scatter in the liquid solvent data, the change of frequency with $f_1(n_D^2)$ appears to be larger than anticipated based on the liquid solvent data. The case is most convincing for PEA, where, as a result of higher solubility, the data extend over a much wider range of $f_1(n_D^2)$. However, the TPP data are quite similar to the PEA data where they overlap, and it therefore seems reasonable to suppose that comparably large deviations from the liquid correlations would be observed at lower CO_2 densities if spectra were observable there. (Similar comments apply to BTBP, which is even less soluble in CO_2 than TPP.) On the basis of previous studies of spectral shifts in supercritical fluids, it is natural to ascribe the deviations observed from the liquid solvent correlations to the operation of local density augmentation in the supercritical solvent. Some evidence for this assignment comes from the observation that a similar spectral series of PEA in supercritical CO_2 at a higher temperature (50 °C) shows considerably smaller deviations from those illustrated here. We will estimate the extent of this local density augmentation using the deviations from the $f_1(n_D^2)$ correlations shown in Figure 7 after discussing the observed rotational dynamics.

B. Fluorescence Lifetimes and Rotation Times. The emission decays observed at magic angle polarization, corresponding to the population ("*m(t)*") decay times, were in the range 2.5−5.5 ns for all probe/solvent combinations. As already discussed in section III.B, with the exception of a small

TABLE 3: Summary of Rotational Data in Liquid Solvents at 295 K[a]

		TPP			PEA			BTBP[c]		
solvent	η^b (cP)	$r(0)$	τ_{rot} (ps)	C_{obs}	$r(0)$	τ_{rot} (ps)	C_{obs}	$r(0)$	τ_{rot} (ps)	C_{obs}
Nonpolar Solvents										
2-methylbutane	0.22	0.38	48	0.84	0.37	45	0.72			
n-hexane	0.29	0.36	65	0.86	0.35	54	0.64	0.33	170	1.06
cyclohexane	0.90	0.37	184	0.79	0.38	144	0.56			
n-decane	0.90	0.36	185	0.80	0.28[d]	144	0.56	0.365	430	0.94
decalin	2.42	0.37	508	0.78	0.28[d]	348	0.50			
n-hexadecane	3.04	0.35	613	0.82	0.38	434	0.51	0.367	1380	0.83
Polar Aprotic Solvents										
acetone	0.30	0.38	66	0.85	0.38	60	0.70			
acetonitrile	0.34	0.37	70	0.80	0.39	56	0.58			
THF	0.46				0.37	88	0.60			
benzene	0.60	0.36	126	0.81	0.38	103	0.65			
DMF	0.80	0.38	167	0.81	0.38	148	0.68			
DMSO	1.99	0.36	440	0.86	0.38	383	0.58			
Associated Solvents										
methanol	0.55	0.39	100	0.70	0.38	92	0.59	0.40	250	0.83
ethanol	1.08	0.36	188	0.68	0.38	136	0.44	0.377	640	1.12
n-propanol	1.94	0.35	329	0.66	0.38	221	0.40	0.382	900	0.83
n-pentanol[e]	3.51	0.35	563	0.62	0.36	379	0.38	0.369	1650	0.89
n-decanol[e]	10.9	0.34	1850	0.65	0.35	1165	0.37	0.365	5500	0.82
formamide	3.30	0.37	650	0.77	0.38	544	0.67			

[a] Data reported here were obtained from iterative reconvolution fits to magic, parallel, and perpendicular decays. $r(0)$ was freely varied in these fits. Uncertainties in $r(0)$ are ± 0.01 and for rotation times are on the order of $\pm 5-15\%$. [b] Viscosity values are interpolated from tabulations in Riddick, J. A.; Bunger, W. B.; Sakano, T. K. *Organic Solvents*; Wiley: New York, 1986. [c] BTBP data in nonpolar and associated solvents were taken from ref 43. [d] These $r(0)$ values were recovered from measurements using 385 nm excitation. [e] The rotation times in these solvents were biexponential for TPP and PEA. These reported times reflect the average rotation time.

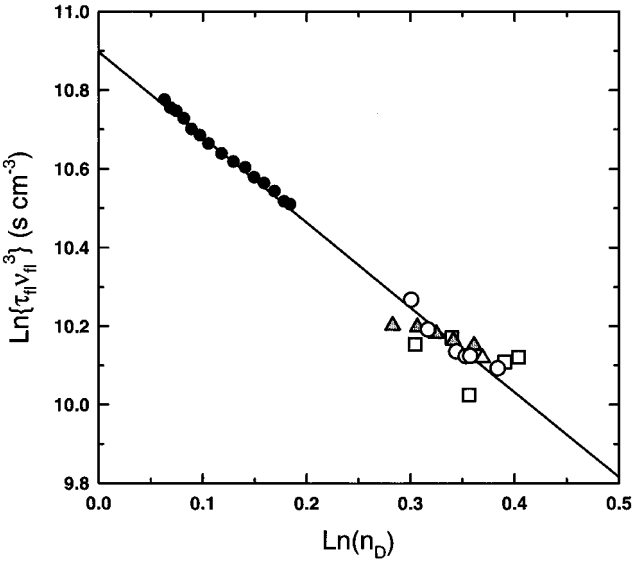

Figure 8. Fluorescence decay times (approximately equal to radiative lifetimes) of PEA in liquid solvents and supercritical CO_2 versus solvent refractive index. Lifetimes are multiplied by the cube of the average emission frequency, and a log−log representation is used to illustrate adherence to eq 8. The large symbols represent each of the solvent classes used in these experiments: nonpolar (○), polar aprotic (□), and polar protic (alcohols, ▲). (The liquid solvents represented here correspond to those listed in Table 3). The supercritical CO_2 data (●) is at $T_r = 1.01$. The solid line is a linear regression to all of the liquid and supercritical CO_2 data.

scattering artifact in the supercritical cell, all magic angle decays were found to be single-exponential functions of time. No unusual behavior of the lifetimes was observed in the supercritical CO_2 samples. As an example, Figure 8 shows the results for PEA in CO_2 and in liquid solvents. Although we have not measured quantum yields in the present study, the quantum yield of PEA is believed to be near unity in all solvents.[63,64] The fluorescence lifetimes therefore provide good approximations for the radiative lifetimes τ_{rad}. Our choice of format for Figure 8 is based on the expectation that the radiative lifetimes should depend on the refractive index (n_D) and emission frequency in a given solvent via a relation of the general form

$$\tau_{rad}^{-1} \propto f(n_D)\nu_{fl}^{3} \cong n_D^{p}\nu_{fl}^{3} \qquad (8)$$

There are a variety of predictions for the function $f(n_D)$,[65] but if one assumes the transition moment is independent of solvent, over the relevant range of n_D, an approximate power law with $2 \geq p \geq 3$ is predicted by the majority of approaches. In the present case, Figure 8 shows that the data are well fit by such a law with a power $p \cong 2$. Apart from the much larger scatter among the liquid solvents, the behavior in CO_2 is consistent with the behavior in typical liquids. Thus, if only the CO_2 data are fit, one finds $p = 2.13 \pm 0.04$ with $R = 0.997$, and if the liquid solvent data are included, the best fit is nearly identical, $p = 2.16 \pm 0.06$ with $R = 0.989$. This behavior is consistent with the results of one liquid phase study of PEA,[63] which also found a squared dependence of the lifetime on n_D. Our results differ slightly from those recently published by Sun and coworkers, who reported $p = 2.86$ for PEA in supercritical CO_2 at 35 °C.[44] The reasons for this difference are unclear.[66] It is interesting to note that local density augmentation apparent from the frequency shifts of PEA in CO_2 appears to have little effect on its lifetimes. If an effective local index of refraction is calculated from what the apparent $f_1(n_D^2)$ reported by the spectral shifts, one would predict a much different lifetime dependence on density than that which is actually observed. It may be that the main effect of the index of refraction entails interactions over distances comparable to the wavelength of the radiation involved.[67] If this were the case, the density enhancement sensed by the spectral shifts (which are determined by a very small region surrounding the solute) might be expected to have a negligible effect on the radiative rates.

We now turn to a consideration of the rotation times of the three solutes in both supercritical CO_2 and in typical liquid solvents. The relevant data are summarized in Tables 3 and 4

TABLE 4: Summary of Solvent Properties, Rotation Times, and Coupling Factors, for Experiments in Supercritical CO_2

pressure (psia)	reduced density (ρ/ρ_r)	viscosity (μP)	τ_{rot}[a] (ps)	C_{obs}
		TPP (308 K)		
1200	1.16	398	8.9	0.90
1250	1.31	466	11.3	0.98
1300	1.39	505	11.4	0.90
1600	1.57	620	15.8	1.02
2500	1.78	786	14.9	0.76
3500	1.90	909	19.7	0.87
		PEA (308 K)		
1120	0.66	235	11.2	1.64
1150	0.80	270	15.3	1.95
1170	0.95	319	13.9	1.50
1190	1.11	374	16.9	1.55
1230	1.27	445	16.4	1.27
1300	1.39	505	17.1	1.16
1600	1.57	620	21.9	1.22
2200	1.73	741	21.4	1.00
3000	1.90	909	24.3	0.92
		BTBP (308 K)		
1300	1.40	510	28	1.10
1400	1.48	559	32	1.14
1500	1.54	595	34	1.14
2200	1.73	743	43	1.16
		BTBP (310 K)		
1270	1.21	418	23	1.11
1400	1.41	518	25	0.97
1500	1.48	560	28	1.00
1700	1.57	620	36	1.17
2200	1.70	720	40	1.12
3000	1.83	833	47	1.13

[a] Densities and viscosities were calculated as described in section II (see refs 46−48). [b] Rotation times reported here are averages of the iterative reconvolution and integration fits to the polarized emission decays. Uncertainties in the rotation times are on the order of ±10−25%. See section III-B for further details. Note: The $r(0)$ values for each probe were fixed in these fits using the results obtained in the liquid fits.

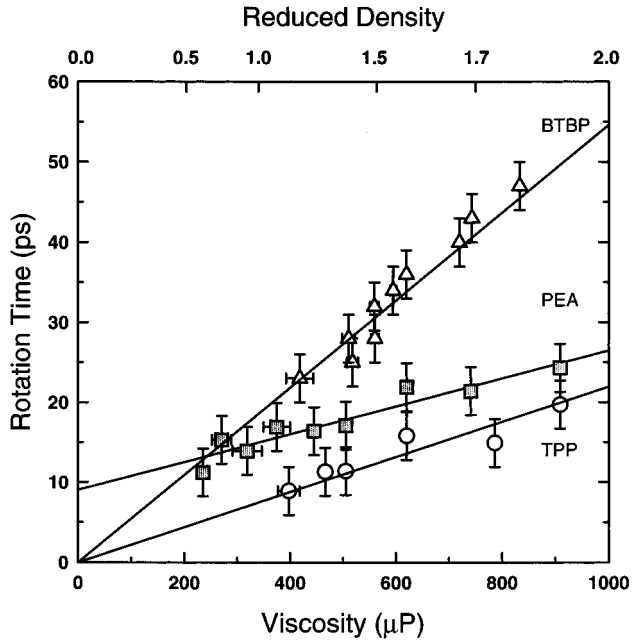

Figure 9. Rotation times of TPP (○), PEA (■), and BTBP (△) in supercritical CO_2 as a function of fluid viscosity. The solid lins are linear regressions to each data set. For convenience, the upper axis shows the corresponding reduced density scale.

and plotted in Figures 9−12. In nearly all cases the anisotropy decay functions ($r(t)$) could be well fit by monoexponential

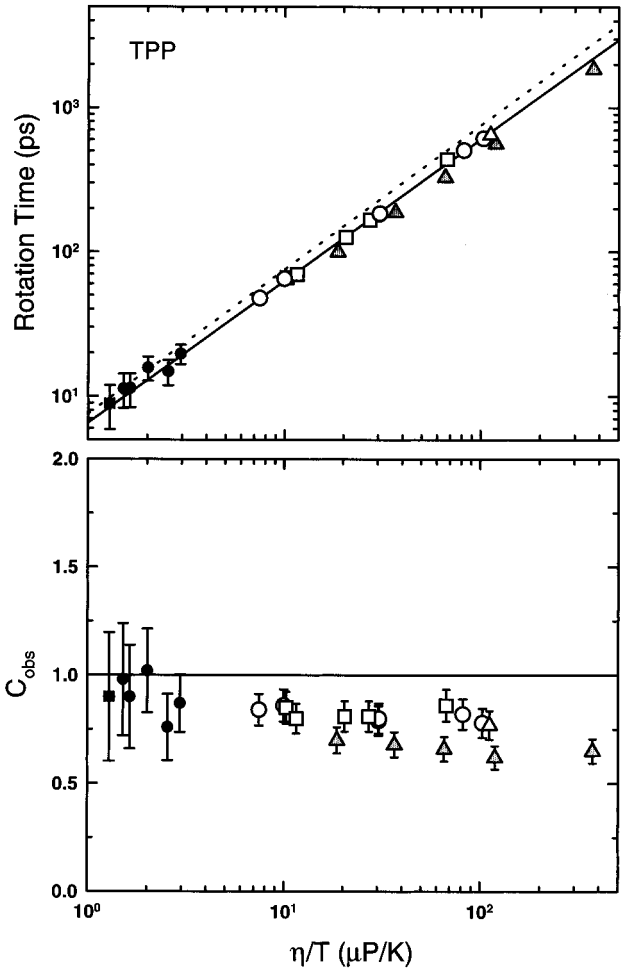

Figure 10. Upper panel: Rotation times of TPP in liquids at 295 K (○, nonpolar; □, polar aprotic; ▲, polar protic) and supercritical CO_2 at 308 K (T_r = 1.01, ●) as a function of viscosity/temperature. The solid line is a linear regression generated using the liquid nonpolar and polar aprotic data. The dashed line illustrates the stick hydrodynamic prediction for TPP according to eq 1 (see Table 1 for specific values). Lower panel: Corresponding C_{obs} calculated using eq 6 as a function of viscosity/temperature.

functions of time, as would be anticipated from the stick hydrodynamic calculations on ellipsoidal bodies (Table 1).[68] However, in four cases, the solutes TPP and PEA in the solvents pentanol and decanol, a biexponential $r(t)$ was required to fit the data adequately. These few instances of nonexponential anisotropies are probably due to time-dependent friction effects in these slowly relaxing solvents. Such behavior has been discussed in detail with respect to another solute, coumarin 153, in previous work.[58] For the purposes of the present study, we will ignore this interesting aspect of the data and only report the average rotation times, determined from the anisotropy fits by $\sum_i b_i \tau_{rot,i}$ (see eq 3).

The rotation times measured for the three probes in supercritical CO_2 are compared in Figure 9. The symbols represent the measured times and the solid lines represent the best linear fits to the data as a function of viscosity. Two features of the rotation times are apparent in Figure 9. First, at a given bulk CO_2 density (or viscosity) the probe order with respect to rotation time is TPP < PEA < BTBP. This ordering is consistent with the hydrodynamic predictions listed in Table 1. For BTBP and TPP the expected proportionality between τ_{rot} and η is observed to within the uncertainties in the data. (Inclusion of a nonzero intercept in these cases yields no better fit.) In contrast, in the case of PEA a large (9 ps)

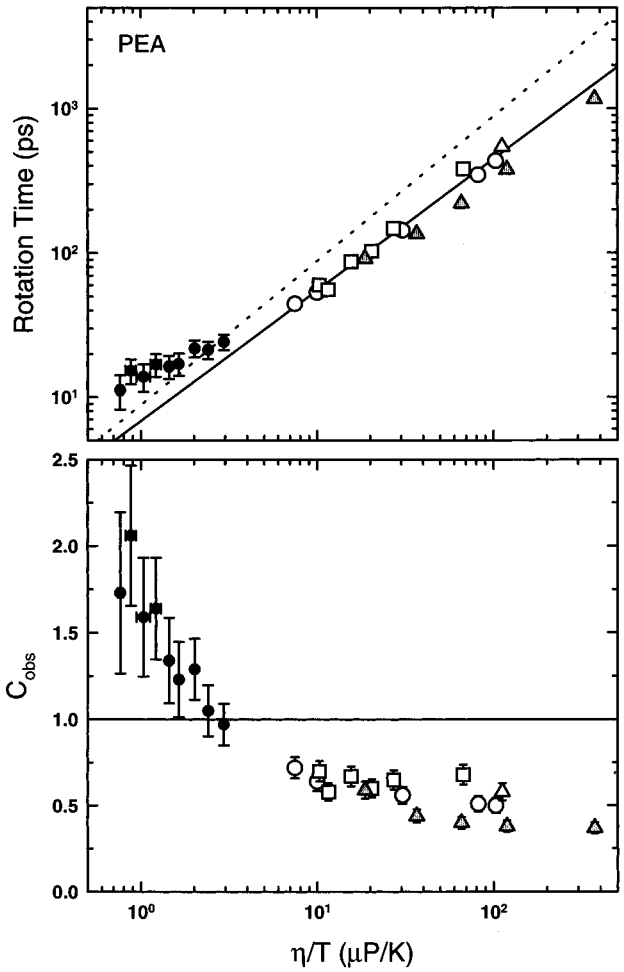

Figure 11. Upper panel: Rotation times of PEA in liquids at 295 K (○, nonpolar; □, polar aprotic; ▲, polar protic) and supercritical CO_2 at 308 K ($T_r = 1.01$, ●) as a function of viscosity/temperature. The solid line is a linear regression generated using the liquid nonpolar and polar aprotic data. The dashed line illustrates the stick hydrodynamic prediction for PEA according to eq 1 (see Table 1 for specific values). Lower panel: Corresponding C_{obs} calculated using eq 6 as a function of viscosity/temperature.

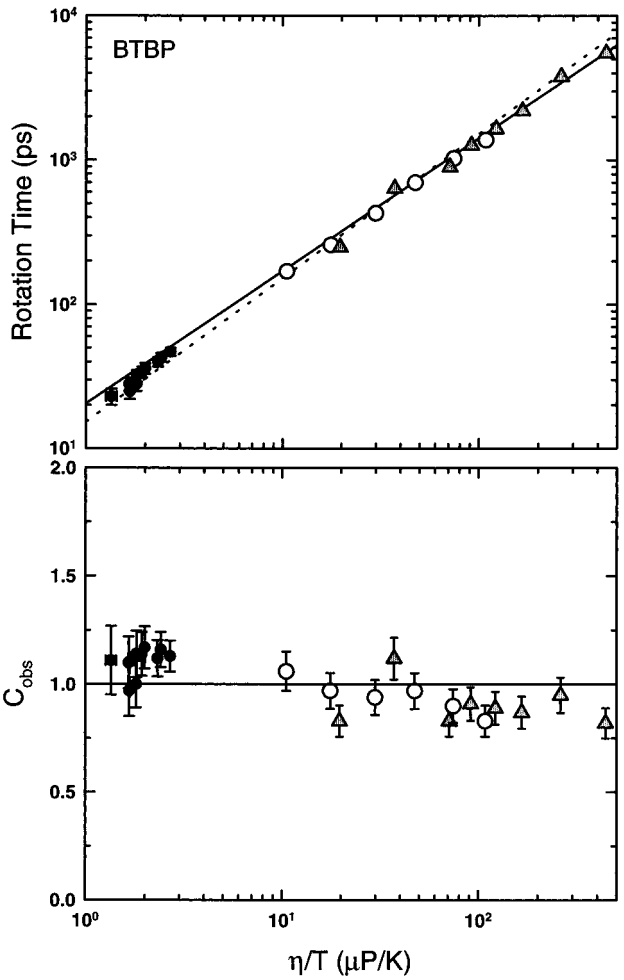

Figure 12. Upper panel: Rotation times of BTBP in liquids (○, nonpolar; ▲, polar protic from ref 43) and supercritical CO_2 at 308 and 310 K ($T_r = 1.01$, ●) as a function of viscosity/temperature. The solid line is a linear regression generated using all of the liquid results. Ben-Amotz and Drake[43] show that BTBP displays the same behavior as a function of viscosity/temperature in both alkane and alcohol solvents; thus we include alcohols in calculating the regression. See text for further details. The dashed line illustrates the stick hydrodynamic prediction for BTBP according to eq 1 (see Table 1 for specific values). Lower panel: Corresponding C_{obs} calculated using eq 6 as a function of viscosity/temperature.

nonzero intercept is required to adequately describe the data. Given the very low viscosities in supercritical CO_2, one might be tempted to assign this nonzero intercept to the zero-viscosity limit, "free rotor time" of the solute. However, 9 ps is a factor of 3 greater than the inertial rotation time calculated for PEA (see Table 1). In addition, it is probably unrealistic to think that the zero-viscosity limit is approached by any of these large solutes at the experimentally observable densities. Rather, as we will show, it is more reasonable to ascribe this non-hydrodynamic behavior to changes in the solute−solvent coupling as a function of fluid density.

In order to decide what the behavior of PEA (and the other solutes) might be telling us about the SCF environment, it is necessary to view these results against a backdrop of the rotation times measured in more usual, liquid solvents. This is accomplished in Figures 10−12. Consider first the upper panels of these figures, in which rotation times are plotted versus viscosity in a double-logarithmic representation. As in previous figures, the different symbols used here denote different solvent classes: nonpolar (open circles), polar aprotic (squares), polar protic (triangles), and supercritical CO_2 (filled circles). The dashed lines are the stick hydrodynamic predictions and the solid lines represent the following linear regressions to the log−log data in liquid solvents only:

$$\text{TPP: } \tau_{rot} = (6.76 \pm 0.05)\{\eta/T\}^{0.98\pm0.02}$$
(protic solvents excluded; $N = 13$, $R = 0.999$)

$$\text{PEA: } \tau_{rot} = (7.38 \pm 0.07)\{\eta/T\}^{0.87\pm0.02}$$
(protic solvents excluded; $N = 12$, $R = 0.999$)

$$\text{BTBP: } \tau_{rot} = (16.9 \pm 0.3)\{\eta/T\}^{0.95\pm0.03}$$
(all solvents; $N = 12$, $R = 0.997$)

(These fits are for τ_{rot} in ps and η/T in μP/K; uncertainties reflect $\pm1\sigma$, and N and R are, respectively, the number of data points and the correlation coefficient of the regression.) Several features of these results are noteworthy. First, with the exception of PEA, the rotation times in supercritical CO_2 appear to follow a correlation similar to the liquid solvents. For TPP and BTBP the observed behavior in liquids and supercritical CO_2 is approximately what is expected from simple hydrodynamic theories. For example, on the basis of the above correlations the rotation times of TPP and BTBP at 1 cP and 295 K are 214 and 480 ps, which are both within 20% of the stick hydrodynamic estimates given in Table 1. The agreement is consider-

ably worse for PEA, whose "observed" rotation time under these conditions is 158 ps, nearly 50% faster than the stick predictions. But, given the crudity of the ellipsoidal representations employed for these molecules, even this level of disagreement is not surprising and does not necessarily signal a failure of hydrodynamic models. What is more telling is the fact that whereas the rotation times of TPP and BTBP are essentially proportional to solvent viscosity, PEA shows a significant departure from an η^1 law. Similar nonunit power-law behavior has been observed previously in numerous cases.[58,69] As there are fundamental reasons to think that at long range an η^1 dependence must be obeyed,[70] the departures from this expectation are often best viewed as reflecting a change in the nature of the coupling of the solute to its immediate surroundings. It is therefore instructive to switch attention from the rotation times themselves to what we will call the observed coupling factors (C_{obs}) derived from these times via the relation

$$C_{obs} \equiv \frac{\tau_{rot}}{\tau_{stick}} \propto \frac{\tau_{rot}}{\eta/T} \tag{9}$$

Variation of C_{obs} as a function of solvent conditions can be viewed as reflecting changes in the short-range coupling between the solute and different solvents. If one has an accurate calculation of τ_{stick}, then C_{obs} should rigorously approach unity as solvent/solute size ratio approaches zero. Even without such an accurate estimate of τ_{stick} this representation serves to remove the large but uninstructive effect of viscosity so as to allow all solvents and supercritical CO_2 to be compared more directly.

The bottom panels of Figures 10−12 show the observed coupling factors for each probe as a function of viscosity. Departure from a strict proportionality between rotation time and viscosity is signaled by the lack of constancy of C_{obs} in these representations. For all three probes in liquid solvents, one finds a general trend toward decreasing C_{obs} with increasing viscosity. The trend is most evident for PEA, which has the smallest viscosity exponent, but it can also be seen in the other solutes. At least within nonpolar solvents, this behavior can be interpreted as being the result of a decrease in C_{obs} with increasing solvent size.[71] (The apparent dependence of C_{obs} on viscosity is merely a secondary effect of the fact that viscosities tend to increase as the solvent molecule size increases.) In addition to this general trend, these plots also reveal that different solvent classes often exhibit slightly different coupling factors. The differences are largest for PEA, are somewhat smaller for TPP, and are apparently absent in BTBP.[43] In PEA, for a given viscosity, the *n*-alcohol solvents have values of C_{obs} that are ∼40% smaller than those in alkanes of comparable viscosity, which are in turn slightly smaller than values in polar aprotic solvents. In TPP the main difference is between the *n*-alcohols and other solvents. Here, C_{obs} values are again smaller in alcohol solvents than in the other solvent types, in this case by only 15−20%. Such differences, especially the faster rotation times of nonpolar solutes such as PEA and TPP in alcohol solvents, have been noted in many previous studies.[72] These differences, along with the size trends noted above, indicate that rotation times are sensitive to some details of solvent−solute interactions and not merely the bulk solvent viscosity. But fortunately, such differences are not so large that they confound efforts to use liquid phase data to calibrate expectations in supercritical solvents.

Having characterized all three probes in typical liquid solvents, we now therefore ask what should be expected for their rotation times in supercritical CO_2. To compare to the liquid solvents employed above, CO_2 is probably best viewed as lying somewhere in between the nonpolar and polar aprotic classifications.[73] It is for this reason, in the cases of TPP and PEA (Figures 10 and 11), that we use fits to rotation times in both nonpolar and polar aprotic solvents for making extrapolations to the supercritical CO_2 regime. (In BTBP, since alcohol solvents do not appear distinct from the other solvent types, we include them in the correlations as well.) In viewing the C_{obs} comparisons, one should also consider that CO_2 is smaller than most liquid solvents. For example, the smallest of the nonpolar solvents, 2-methylbutane, has roughly 3 times the van der Waals volume of CO_2. On the basis of trends of C_{obs} with solvent-to-solute size ratio established using a wide variety of solutes in nonpolar solvents,[74] we would anticipate that this difference in size should cause C_{obs} in CO_2 to be 10−20% higher than the value observed in 2-methylbutane. This size effect should be greatest for PEA, the smallest solute, and least for BTBP. With these features in mind, one can say that at the highest CO_2 densities (i.e. the highest few η/T points in Figures 10−12) all of the probes behave roughly as expected. The value of C_{obs} in PEA is perhaps slightly larger than anticipated, but, given the greater variability of C_{obs} for this probe in liquid solvents, one could readily ascribe the difference to inaccuracies in the liquid-based predictions. Proceeding to lower CO_2 densities, the rotation times of TPP and BTBP show no clear deviation from hydrodynamic predictions based on the bulk fluid properties. However, in PEA one does observe an obvious departure that is beyond the uncertainties in the rotational measurements. Since the spectral shift data described in section IV-A indicate the presence of significant local density enhancement for this solute, it is reasonable to ascribe this behavior of the rotation times to differences in the properties of the fluid (i.e. "viscosity" and density) in the neighborhood of the solute compared to those in the bulk.

Estimates of the magnitude of the local density enhancement can be made on the basis of both the rotation times and the spectral shifts. As others have done previously, we define the effective local density, ρ_{eff}, determined using some observable property of the solute, p_{obs}, as

$$\rho_{eff}^{(p)} \equiv F^{-1}(p_{obs}) \quad \text{for} \quad p = F(\rho) \tag{10}$$

In these expressions $F(\rho)$ denotes the functional relationship between the observable property p and density in the homogeneous fluid, i.e. what would be observed in the supercritical fluid in the absence of density augmentation.[75] Determining the proper function $F(\rho)$ is not without ambiguity, since we must rely on inexact extrapolations of the liquid-state behavior to the supercritical regime. We allow some flexibility in these extrapolations by assuming

$$\tau_{rot}(\rho) = C\eta(\rho) \tag{11}$$

and

$$\nu(\rho) = \nu_0 + A\left(\frac{n_D^2(\rho) - 1}{2n_D^2(\rho) + 1}\right) \tag{12}$$

with the values of C and ν_0 adjusted slightly from the correlations established in liquid solvents (Figures 7 and 11) so as to reproduce the bulk fluid density at the highest pressures employed.[76] In other words, we assume no local density augmentation at the highest densities. The density enhancements we deduce therefore represent lower bounds to the true values.

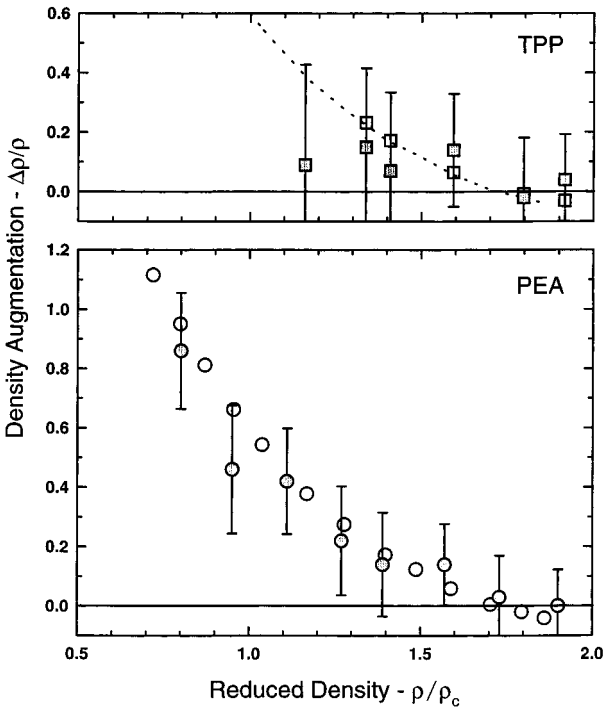

Figure 13. Extent of local density augmentation defined by eq 13 for TPP and PEA in supercritical CO_2 at $T_r = 1.01$. In both panels the open symbols show estimates based on steady-state frequency shifts, whereas the solid symbols depict values calculated using the rotation times. The dashed line in the upper panel (TPP data) denotes the augmentation observed for PEA. It is included here to suggest that the local density augmentation in TPP may in fact be similar to that in PEA, only more difficult to measure due to the lower solubility of TPP in CO_2.

The local density augmentation factors,

$$\frac{\Delta\rho}{\rho} \equiv \frac{\rho_{\text{eff}} - \rho}{\rho} \tag{13}$$

obtained in this manner are shown in Figure 13. The open symbols denote values determined from the spectral shifts, and the solid symbols those from the rotation times. The primary data are for PEA, shown in the bottom panel of Figure 13. The local density enhancements deduced for this solute are appreciable even at densities above the critical density. By a reduced density of 0.7 (the solubility limit for PEA) the enhancement is slightly larger than a factor of 2. This value is comparable to the maximal enhancement factors deduced by others from spectroscopic shifts of various solutes in supercritical CO_2. What is most interesting about these data is the fact that both the rotation times and the spectral shifts in PEA provide the same values of ρ_{eff} to within experimental uncertainties. This behavior, while not unexpected, is far from necessary. Rotational motion and the transition energies of the solute monitor its local environment in distinct ways. In particular the length scales on which the surroundings are sensed may be different in the two cases so that it is not obvious that the effective densities they report should be the same.

Finally, we would like to point out that while the rotational behavior of PEA may appear unlike that of the other two probes employed here, the distinction is probably only a result of the lower solubility of TPP and BTBP. Some evidence for this idea is provided in the top panel of Figure 13, where we have plotted the results of the above analysis performed with the limited TPP data available. It is clear from this data that the range of observable densities is too small and the uncertainties in the rotation times too large to put much confidence in the values determined. However, the comparison between these values of the local density augmentation and the PEA results (dashed curve) suggests that similar local density augmentation effects might be observable in these other solutes if the solubility did not prevent access to lower CO_2 densities. Thus, the rotational behavior of PEA is probably in no way unusual, only more readily measured in the relevant regions of the supercritical fluid.

V. Summary and Conclusions

In this paper we have examined the solvatochromic shifts and rotational dynamics of TPP, PEA, and BTBP in typical liquid solvents and supercritical CO_2. The main results of this study may be summarized as follows. Steady-state spectroscopy of all three probes in simple liquid solvents shows that solvation is dominated by the electronic polarizability of the solvent and not its permanent charge characteristics. In supercritical CO_2 at high density, the spectral shifts are consistent with correlations to solvent dielectric properties established in liquid solvents (Figure 7). However, at sufficiently low CO_2 densities ($\rho_r \approx 1$), a clear departure from the liquid phase correlations is observed. Such departures have been noted many times previously,[5,8,12−19,37] and they provide one means for quantifying the extent of local density augmentation present in these systems. The most definitive data is obtained with the solute PEA, which is soluble in supercritical CO_2 to much lower densities than the other two solutes. At 35 °C ($T_r = 1.01$) the spectral shifts yield estimates of ∼100% local density augmentation ($\Delta\rho/\rho$) near ρ_r ∼0.8, the lowest density observable. We note that the augmentation effect is greatly reduced ($\Delta\rho/\rho \approx 50\%$) upon raising the temperature to 50 °C. Spectroscopic signatures of local density augmentation are less obvious for the other two probes.

The rotational dynamics observed for all three solutes in liquid solvents are in rough accord with the expectations of hydrodynamic theories. Thus, rotation times in different solvents are approximately proportional to solvent viscosity, and they lie within a factor of 2 of predictions based on ellipsoidal representations of the molecular shape and stick boundary conditions (Table 1). Some deviations from simple hydrodynamic behavior are observed, but such predictions nevertheless provide a reliable guide to what to expect in supercritical solvents. In TPP and BTBP the rotation times observed in supercritical CO_2 are consistent with extrapolations of the liquid solvent behavior to the lower viscosities present in the supercritical solvent. In the case of PEA, rotation times in CO_2 clearly depart from the anticipated behavior. With decreasing CO_2 density (viscosity), the rotation times of PEA decrease, as would be expected, but not in proportion to the decrease in the bulk solvent viscosity (Figure 11). This departure from simple hydrodynamic behavior is undoubtedly related to the density augmentation present in the supercritical solvent. Estimates of the effective local density based on the observed rotation times of PEA are indistinguishable from the estimates made based on the electronic spectral shifts (Figure 13). Thus, in PEA at least, one finds that the magnitude of the local density augmentation reported by the electronic spectra (or solvation energies) of the solute are approximately the same as those reflected in its rotational dynamics. This similarity, as well as the extent of augmentation observed here, is comparable to results recently reported in the case of vibrational spectral shifts and vibrational relaxation times of the solute $W(CO)_6$.[33] However, it is worth noting again that while the similarity between static and dynamic measures of augmentation provided by these two cases seems gratifying, it is not a foregone

conclusion. Electronic spectral shifts and rotational friction are distinct observables that may be impacted by solute−solvent interactions occurring on different length scales. It would therefore not be surprising to have them report different local densities, since such "densities" are after all mainly a heuristic device. As mentioned in connection with Figure 8, the radiative rates of PEA, yet another observable, would report negligible local density augmentation for this same molecule. Finally, we should remark that although we do not see clear indications of the effects of local density augmentation on the rotation times of the solute TPP and BTBP, it is probably only a result of the fact that we were unable to study them to sufficiently low densities. (See the top panel of Figure 13.)

We now consider the present results in light of prior studies of rotational dynamics in supercritical fluids. The results obtained here are most similar to those obtained by Anderton and Kauffman.[39] These authors reported decreasing rotation times with decreasing solvent density and relatively small effects of local density enhancement on rotation times. On the basis of a free-volume theory of rotational dynamics[42] and assuming that the rotation times observed in supercritical fluids extrapolate to free rotor times, they concluded that diphenylbutadiene (DPB) rotations do not show the effects of local density augmentation (for $\rho_r \geq 0.9$) in CO_2, whereas 4-hydroxymethylstilbene (HMS) rotation times do. In the latter case they estimated an approximately constant local density augmentation of 30−40% for all densities greater than $\rho_r \approx 0.6$. We note that had the present methods of analysis been applied to the data of Anderton & Kauffman, somewhat different conclusions as to the extent of local density augmentation would have been reached for these two solutes.[77] Nevertheless, either analysis would indicate departures from "expected" hydrodynamic behavior which could be reasonably explained on the basis of local densities being higher than bulk densities by an amount comparable to what has been reported in most spectroscopic studies. Thus, our results are in reasonable agreement with those of Anderton and Kauffman.[39]

In contrast, our results differ markedly from the findings of Bright and co-workers.[37,38] For two different solutes, PRODAN and BTBP, in several supercritical solvents, Bright and co-workers reported rotation times to increase as density is decreased from high density toward ρ_c. Our data on BTBP in CO_2 (Figure 9) can be directly compared to some of their results (Figure 5 of ref 38). While the two sets of data agree at the highest densities, they show completely opposite trends with density. In order to compare with this earlier work in more detail, we have also measured rotation times of BTBP in supercritical CF_3H.[78] These additional measurements yield comparisons very similar to the CO_2 case reported here. Rather than the ∼8-fold increase in rotation time observed by Heitz and Bright,[38] we find a decreasing rotation time with density, with the decrease being nearly proportional to the bulk viscosity of the solvent. Thus, the present results are at odds with the findings of these earlier studies, and we must ask two questions: (i) which (if either) set of data is to be believed, and (ii) what is the source of this discrepancy? As far as the first question goes, the present data would seem preferable, based simply on the fact that they can be understood in terms of the same sorts of local density augmentation observed in a variety of other near critical situations. On the other hand, it is difficult to imagine the physical basis for rotation times (rotational friction) increasing as one lowers the density of the surrounding fluid. This is especially true since the anomalous behavior reported by Bright and co-workers occurs at densities that are well removed from ρ_c and thus cannot be rationalized on the basis of the critical slowdown that occurs very close to the critical point.[79]

Why then the difference between the two sets of results? We first note that one major difference between the two sets of experiments is that Bright and co-workers[37,38] used frequency-domain modulation spectroscopy, whereas the present experiments are conducted in a time-domain mode.[80] While the two methods contain identical information in principle, they may be differentially sensitive to various experimental artifacts. After a detailed examination of the two experiments, we suggest that one plausible explanation for the unusual rotation times determined from the frequency-domain data may be due to the use of emission wavelengths which inadvertantly included regions of significant Raman scattering from solvent vibrational modes.[38] From time-domain experiments it is clear that emission collected over regions containing solvent Raman bands should be significantly distorted by this Raman contribution, especially at low densities where fluorescence emission is weak. Since the amount of BTBP solubilized decreases markedly at lower densities (see, for example, the inset to Figure 6), the relative contribution of this fast scattering component increases with decreasing density. In a time-domain experiment this scattering component is clearly revealed by a prominent spike near zero time. However, its effect in the frequency-domain measurements is more insidious. Scattering is manifest as a systematic deviation in the frequency dependence of the phase angle and modulation ratio from their true values.[81] Numerical simulations of anisotropy data demonstrate that the deviations so produced are in the correct direction to qualitatively reproduce the density-dependent behavior of the differential polarized phase and polarized modulation ratio.[82] Confirmation of this hypothesis awaits further frequency-domain experiments, which we hope to undertake in the near future.[83]

In conclusion, the present results indicate less dramatic effects of local density augmentation on rotational dynamics than had been reported in some past studies.[37,38] Taken together, the data reported here and most other data available on the rotations of probe solutes and on other nonreactive dynamics[31−33,36,39] provide the following tentative picture. Local density augmentation leads to increased friction and thereby retards solute dynamics to an extent that is approximately commensurate with its effect on solvation energetics (spectral shifts). The effect of local density augmentation on solvent friction generally seems to account for at most a factor of 2−3 increase in the friction over the value expected from bulk solvent properties alone. Maximal effects are observed for temperatures near to T_c ($T_r <$ 1.1) and for densities below the critical density ($\rho_r \approx 1/2$). We would expect these observations to also apply to the effect of local density augmentation on the solvent friction operative in reactive situations. However, the case of reactions can be much more complicated,[84] and a good deal more study of both reactive and nonreactive systems will be needed to demonstrate the generality of these observations.

Acknowledgment. The authors would like to acknowledge helpful discussions with Frank Bright on the possible sources of the different rotation times measured for BTBP and Abby Robinson for assistance in obtaining some of the steady-state spectra reported here. This work was supported by a grant from the Office of Naval Research.

Appendix

In this appendix we describe a method for determining rapid rotation times from time-resolved data which does not involve iterative reconvolution fitting. The underlying idea is to

numerically integrate the difference between the parallel and perpendicular emission decays in order to determine the integral (or correlation) time of *r(t)*. Since it is this correlation time that is often of most interest, the method may be advantageous in cases where accurate deconvolution of the instrumental response function is difficult.

Let $i_{||}(t)$ and $i_{\perp}(t)$ denote the hypothetical emission decays that would be observed with an ideal instrument. They are related to the ideal population (*m(t)*) and anisotropy (*r(t)*) decay functions via the relations

$$i_{||}(t) = m(t)\{1 + 2r(t)\} \qquad i_{\perp}(t) = m(t)\{1 - r(t)\} \quad \text{(A.1)}$$

or

$$m(t) = {}^1/_3\{i_{||}(t) + 2i_{\perp}(t)\} \qquad r(t) = \frac{i_{||}(t) - i_{\perp}(t)}{i_{||}(t) + 2i_{\perp}(t)} \quad \text{(A.2)}$$

Letting *s(t)* denote the instrument response function, the emission signals actually observed ($I_x(t)$) are convolutions of these ideal decays,

$$I_{||}(t) = \int_0^{\infty} s(t - \tau)\, i_{||}(t)\, \mathrm{d}\tau + b_{||}$$

and

$$I_{\perp}(t) = g^{-1} \int_0^{\infty} s(t - \tau)\, i_{\perp}(t)\, \mathrm{d}\tau + b_{\perp} \quad \text{(A.3)}$$

where b_x denotes the background level (i.e. the signal level detected prior to the excitation pulse) and g is the polarization bias of the detection system:

$$g = \lim_{t \to \infty} \frac{I_{||}(t) - b_{||}}{I_{\perp}(t) - b_{\perp}} \quad \text{(A.4)}$$

To determine the characteristics of *r(t)* from these observed signals, we first calculate the sum $M(t)$ and difference $D(t)$ functions defined by

$$D(t) \equiv {}^1/_3\{[I_{||}(t) - b_{||}(t)] - g[I_{\perp}(t) - b_{\perp}(t)]\} = \int_0^{\infty} s(t - \tau)\, m(t)\, r(\tau)\, \mathrm{d}\tau \quad \text{(A.5)}$$

and

$$M(t) \equiv {}^1/_3\{[I_{||}(t) - b_{||}(t)] + 2g[I_{\perp}(t) - b_{\perp}(t)]\} = \int_0^{\infty} s(t - \tau)\, m(t)\, \mathrm{d}\tau \quad \text{(A.6)}$$

To determine *r(t)*, one must deconvolute the effect of the instrument response function *s(t)* from *D(t)* and *M(t)*. This deconvolution may be performed directly using Fourier transform techniques. However, because such methods suffer severe numerical instabilities at the noise levels typical in TCSPC, most practitioners determine *r(t)* via iterative reconvolution fitting.[50,56] Such fitting is time consuming and, for very rapid anisotropy decays, relies on having an accurate representation of the instrumental response function *s(t)*. In the case of SCF data it may be difficult to obtain sufficiently good response functions to be able to fit the anisotropy data with confidence.

However, if one does not need *r(t)* itself but rather only its correlation time,

$$\tau_{\mathrm{rot}} \equiv \int_0^{\infty} \frac{r(t)}{r(0)}\, \mathrm{d}t \quad \text{(A.7)}$$

a simpler method, which does not rely on an accurate determination of *s(t)*, can be employed. Consider the time integral of the difference function:

$$\int_0^{\infty} D(t)\, \mathrm{d}t = \int_0^{\infty} \mathrm{d}t \int_0^{\infty} s(t - \tau)\, m(t)\, r(\tau)\, \mathrm{d}\tau = \int_0^{\infty} m(t)\, r(\tau)\, \mathrm{d}\tau \int_0^{\infty} s(\lambda)\, \mathrm{d}\lambda \quad \text{(A.8)}$$

(The last equality here follows from the causality condition $s(t) = 0$ for $t < 0$.) Assume that, at least over the time regime where *r(t)* and *s(t)* are nonzero, the population decay law can be represented by a monoexponential function of time,

$$m(t) = m(0) \exp(-t/\tau_{\mathrm{fl}}) \quad \text{(A.9)}$$

Also assume for the moment that *r(t)* is a monoexponential function. The integral of *D(t)* can then be related to the rotational correlation time of interest by

$$\tau_{\mathrm{D}} \equiv \frac{\int_0^{\infty} m(t)\, r(\tau)\, \mathrm{d}\tau}{m(0)\, r(0)} = \frac{\int_0^{\infty} D(t)\, \mathrm{d}t}{r(0)\, m(0) \int_0^{\infty} s(\lambda)\, \mathrm{d}\lambda} = 1/\tau_{\mathrm{fl}} + 1/\tau_{\mathrm{rot}} \quad \text{(A.10)}$$

Thus the rotation time can be obtained from the difference integral if $r(0)$ and the product $m(0)\int s(\lambda)\, \mathrm{d}\lambda$ are known. We will assume that $r(0)$ is known from other sources such as studies on more viscous solvents. Thus, it only remains to determine $m(0)\int s(\lambda)\, \mathrm{d}\lambda$ from the experimental data. If the instrument response function is sufficiently narrow relative to the decay of *m(t)*, this product is simply the maximum value of the observed *M(t)* function. In such an instance, one does not need to know the instrument response at all in order to determine the rotation time. However, in the cases we have examined in our laboratory, the presence of a small but long-lived tail in *s(t)* renders this simple approximation inaccurate (>10% error). We have therefore found it necessary to evaluate this factor by integrating *s(t)* in the following manner. First we note that *M(t)* can be written in the form

$$M(t) = m(0) \int_0^{\infty} s(t - \tau) \exp(-\tau/\tau_{\mathrm{fl}})\, \mathrm{d}\tau = m(0) \exp(-t/\tau_{\mathrm{fl}}) \int_{-\infty}^{t} s(\lambda) \exp(+\lambda/\tau_{\mathrm{fl}})\, \mathrm{d}\lambda \quad \text{(A.11)}$$

For times after the decay of *s(t)*, $t > t_s$, *M(t)* becomes

$$M(t > t_s) = m(0) \exp(-t/\tau_{\mathrm{fl}}) \int_0^{\infty} s(\lambda) \exp(+\lambda/\tau_{\mathrm{fl}})\, \mathrm{d}\lambda \quad \text{(A.12)}$$

Thus, the product $m(0)\int s(\lambda)\mathrm{d}\lambda$ and therefore τ_{rot} can be determined from the relation

$$\tau_{\mathrm{D}} = \frac{\int_0^{\infty} D(t)\, \mathrm{d}t}{\langle \exp(t/\tau_{\mathrm{fl}})\, M(t) \rangle_{t > t_s} r(0)} \left\{ \frac{\int_0^{\infty} s(t) \exp(t/\tau_{\mathrm{fl}})\, \mathrm{d}t}{\int_0^{\infty} s(t)\, \mathrm{d}t} \right\} \quad \text{(A.13)}$$

where $\langle X(t) \rangle_{t > t_s}$ denotes the value of X averaged over times after the instrument function has completely decayed.

Equations A.10 and A.13 represent the final results of this derivation. These equations allow one to determine τ_{rot} exactly in the case that *r(t)* is a monoexponential function of time. What is required are the observed parallel and perpendicular emission decays and an independent knowledge of *r(0)*. An instrument response function is also needed, but its use here involves only the weighted average (bracketed ratio) in eq A.13, in which it plays the role of a minor correction factor. Thus, an ap-

proximate instrument function, so long as it captures the basic shape of the instrumental response, is sufficient to provide accurate results.

In the above derivation we assumed that *r(t)* was a monoexponential function of time. If *r(t)* is not exponential, the rotation time calculated in this manner is only an approximation to the rotational correlation time. Representing *r(t)* by a multiexponential function,

$$r(t) = r(0)\sum_i a_i \exp(-t/\tau_i) \quad \text{with} \quad \sum_i a_i = 1 \quad \text{(A.14)}$$

the rotation time, T_r, derived from the above method is

$$T_r \equiv (1/\tau_D - 1/\tau_{fl})^{-1} = (\sum_i a_i/\tau_i)^{-1} \qquad \text{(A.15)}$$

whereas the true correlation time defined by eq 7 is $\tau_{rot} = \sum_i a_i\tau_i \leq T_r$. Thus for nonexponential *r(t)*, the time calculated from this procedure yields an upper bound to the true correlation time. (Since the vast majority of time-resolved emission studies do not have sufficient signal-to-noise to detect nonexponentiality in *r(t)*, this feature is hardly a limitation of the method.)

References and Notes

(1) (a) *Supercritical Fluids: Fundamentals for Application*; Kiran, E., Levelt Singers, J. M. H., Eds.; Kluwer: Dordrecht, 1994. (b) *Supercritical Fluid Technology−Reviews in Modern Theory and Applications*; Bruno, T. J., Ely, J. F., Eds.; CRC Press: Boca Raton, FL, 1991. (c) *Applications of Supercritical Fluids in Industrial Analysis*; Dean, J. R., Ed.; CRC Press: Boca Raton, FL, 1993. (d) *Innovations in Supercritical Fluids*; Hutchenson, K. W., Foster, N. R., Eds.; ACS Symposium Series, Volume 608; American Chemical Society: Washington, DC, 1995. (e) *Supercritical Fluid Technology−Theoretical and Applied Approaches in Analytical Chemistry*; Bright, F. V., McNally, M. E. P., Eds.; ACS Symposium Series, Volume 488; American Chemical Society: Washington, DC, 1992. (f) *Supercritical Fluid Engineering Science−Fundamentals and Applications*; Kiran, E., Brennecke, J. F., Eds.; ACS Symposium Series, Volume 514; American Chemical Society: Washington, DC, 1993. (g) *Supercritical Fluid Science and Technology*; Johnston, K. P., Penninger, J. M. L., Eds.; ACS Symposium Series, Volume 406; American Chemical Society: Washington, DC, 1989.

(2) (a) Tester, J. W.; Holgate, H. R.; Armellini, F. J.; Webley, P. A.; Killilea, W. R.; Hong, G. T.; Barner, H. E. In *Emerging Technologies in Hazardous Waste Management III*; ACS Symposium Series, Volume 518; American Chemical Society: Washington, DC, 1993. (b) Brunner, G. H. In *Supercritical Fluids: Fundamentals for Application*; Kiran, E., Levelt Singers, J. M. H., Eds.; Kluwer: Dordrecht, 1994; pp 739−757. (c) Akgerman, A. In *Industrial Environmental Chemistry*; Sawyer, D. T., Martell, A. E., Eds.; Plenum Press: New York, NY, 1992; pp 153−169. (d) Akgerman, A.; Madras, G. In *Supercritical Fluids: Fundamentals for Application*; Kiran, E., Levelt Singers, J. M. H., Eds.; Kluwer: Dordrecht, 1994; pp 669−692.

(3) Brennecke, J. F.; Eckert, C. A. *AIChE J.* **1989**, *35*, 1409. This review provides an overview of much of the early work in this area.

(4) Eckert, C. A.; Ziger, D. H.; Johnston, K. P.; Ellison, T. K. *Fluid Phase Equilib.* **1983**, *14*, 167. See also: Eckert, C. A.; Ziger, D. H.; Johnston, K. P.; Kim, S. *J. Phys. Chem.* **1986**, *90*, 2738.

(5) Johnston, K. P., Kim, S.; Combes, J. In *Supercritical Fluid Science and Technology*; Johnston, K. P., Penninger, J. M. L., Eds.; ACS Symposium Series, Volume 406; American Chemical Society: Washington, DC, 1989. This review as well as the review cited in ref 3 provides a review of early spectroscopic studies.

(6) Sigman, M. E.; Lindley, S. M.; Leffler, J. E. *J. Am. Chem. Soc.* **1985**, *107*, 1471.

(7) Yonker, C. R.; Frye, S. L.; Kalkwarf, D. R.; Smith, R. D. *J. Phys. Chem.* **1986**, *90*, 3022. Smith, R. D.; Frye, S. L.; Yonker, C. R.; Gale, R. W. *J. Phys. Chem.* **1987**, *91*, 3059. Yonker, C. R.; Smith, R. D. *J. Phys. Chem.* **1988**, *92*, 235. Yonker, C. R.; Smith, R. D. *J. Phys. Chem.* **1989**, *93*, 1261.

(8) Kim, S.; Johnston, K. P. *Ind. Eng. Chem. Res.* **1987**, *26*, 1206.

(9) Kajimoto, O.; Futakami, M.; Kobayashi, T.; Yamasaki, K. *J. Phys. Chem.* **1988**, *92*, 1347. Kajimoto, O.; Yamasaki, K.; Honma, K. *Faraday Discuss. Chem. Soc.* **1988**, *85*, 65. Morita, A.; Kajimoto, O. *J. Phys. Chem.* **1990**, *94*, 6420.

(10) See, for example, the reviews: Nicol, M. F. *Appl. Spectrosc. Rev.* **1974**, *8*, 183. Amos, A. T.; Burrows, B. L. *Adv. Quantum Chem.* **1973**, *7*, 289. Mataga, N.; Kubota, T.; *Molecular Interactions & Electronic Spectra*; Mercel Dekker: New York, 1970. Suppan, P. *J. Photchem. Photobiol. A* **1990**, *50*, 293.

(11) For example, refs 12−14 use the intensity ratio between of two vibronic peaks in the emission spectrum of pyrene, the so-called "Ham effect", as the spectroscopic observable.

(12) (a) Brennecke, J. F.; Tomasko, D. L.; Peshkin, J.; Eckert, C. A. *Ind. Eng. Chem. Res.* **1990**, *29*, 1682. (b) Zhang, J.; Lee, L. L.; Brennecke, J. F. *J. Phys. Chem.* **1995**, *99*, 9268.

(13) Sun, Y. P.; Bunker, C. E.; Hamilton, N. B. *Chem. Phys. Lett.* **1993**, *210*, 111.

(14) Rice, J. K.; Niemeyer, E. D.; Dunbar, R. A.; Bright, F. V. *J. Am. Chem. Soc.* **1995**, *117*, 5832.

(15) Sun, Y.-P.; Fox, M. A.; Johnston, K. P. *J. Am. Chem. Soc.* **1992**, *114*, 1187.

(16) Sun, Y. P.; Bunker, C. E. *Ber. Bunsen-Ges. Phys. Chem.* **1995**, *99*, 976.

(17) Bennett, G. E.; Johnston, K. P. *J. Phys. Chem.* **1994**, *98*, 441.

(18) Rice, J. K.; Niemeyer, E. D.; Bright, F. V. *J. Phys. Chem.* **1996**, *100*, 8499.

(19) Carlier, C.; Randolph, T. W. *AIChE J.* **1993**, *39*, 876. Ganapathy, S.; Carlier, C.; Randolph, T. W.; O'Brien, J. A. *Ind. Eng. Chem. Res.* **1996**, *35*, 19.

(20) Debenedetti, P. G. *Chem. Eng. Sci.* **1987**, *42*, 2203.

(21) Cummings, P. T. In *Supercritical Fluids: Fundamentals for Application*; Kiran, E., Levelt Singers, J. M. H., Eds.; Kluwer: Dordrecht, 1994; p 287. Levelt Sengers, J. M. H. *J. Supercrit. Fluids* **1991**, *5*, 192.

(22) Russell, A. J.; Beckman, E. J.; Chaudhary, A. K. *Chemtech* 1994, Mar, 33. Russell, A. J.; Beckman, E. J. *Appl. Biochem. Biotech.* **1991**, *31*, 197.

(23) Beckman, E. J.; Russell, A. J.; Chaudhary, A. K. *J. Am. Chem. Soc.* **1995**, *117*, 3728. Scholsky, K. M. *J. Supercrit. Fluids* **1993**, *6*, 103. Johnston, K. P.; Shim, J.-J. *AIChE J.* **1991**, *37*, 607.

(24) Savage, P. E.; Gopalan, S.; Mizan, T. I.; Martino, C. J.; Brock, E. E. *AIChE J.* **1995**, *41*, 1723.

(25) See the review: Brennecke, J. F. In *Supercritical Fluid Engineering Science−Fundamentals and Applications*; Kiran, E., Brennecke, J. F., Eds.; ACS Symposium Series, Volume 514; American Chemical Society: Washington, DC, 1993; p 201, as well as ref 24 for a discussion of the many solvent influences that must be considered in supercritical fluid reactions.

(26) Brennecke, J. F.; Tomasko, D. L.; Eckert, C. A. *J. Phys. Chem.* **1990**, *94*, 7692.

(27) Zagrobelny, J.; Bright, F. V. *J. Am. Chem. Soc.* **1992**, *114*, 7821. Zagrobelny, J.; Betts, T. A.; Bright, F. V. *J. Am. Chem. Soc.* **1992**, *114*, 5249.

(28) Sun, Y. P.; Bunker, C. E. *J. Phys. Chem.* **1995**, *99*, 13778.

(29) See the reviews: Levelt Sengers, J. M. H.; Deiters, U. K.; Klask, U.; Swidersky, P.; Schneider, G. M. *Int. J. Thermophys.* **1993**, *14*, 893. Liong, K. K.; Wells, P. A.; Foster, N. R. *J. Supercrit. Fluids* **1991**, *4*, 91.

(30) We do not include a discussion of the elegant studies of vibrational relaxation and photodissociation dynamics of I_2 in supercritical rare gases recently published by the Zewail group listed below. All of their experiments lie far from the critical temperatures of the gases so that little information on density augmentation can be obtained these studies. Lienau, C.; Zewail, A. H. *J. Phys. Chem.* **1996**, *100*, 18629. Materny, A.; Lienau, C.; Zewail, A. H. *J. Phys. Chem.* **1996**, *100*, 18650. Liu, Q.; Wan, C.; Zewail, A. H. *J. Phys. Chem.* **1996**, *100*, 18666.

(31) Moustakas, A.; Weitz, E. *Chem. Phys. Lett.* **1992**, *191*, 264.

(32) Pan, X. *Solute-Solvent Interactions and Raman CH Stretching Spectra of Cyclopentane-D9 and Cyclohexane-D11: Bridging the Vapor-Liquid Density Gap*. Dissertation, Duke University, 1995. See also the preliminary account: Pan, X.; MacPhail, R. A. *Chem. Phys. Lett.* **1993**, *212*, 64, which does not discuss augmentation effects.

(33) Urdahl, R. S.; Rector, K. D.; Myers, D. J.; Davis, P. H.; Fayer, M. D. *J. Chem. Phys.* **1996**, *105*, 8973.

(34) We do not discuss studies of rotational dynamics of pure supercritical fluids. However, the recent paper by Okazaki, S.; Matsumoto, M.; Okada, I. *J. Chem. Phys.* **1995**, *103*, 8594, and the early work, Zerda, T. W.; Schroeder, J.; Jonas, J. *J. Chem. Phys.* **1981**, *75*, 1612, are two noteworthy examples of such studies.

(35) Two early NMR studies: Lamb, D. M.; Adamy, S. T.; Woo, K. W.; Jonas, J. *J. Phys. Chem.* **1989**, *93*, 5002. Evilia, R. F.; Robert, J. M.; Whittenburg, S. L. *J. Phys. Chem.* **1989**, *93*, 6550.

(36) Howdle, S. M.; Bagratashvili, V. N. *Chem. Phys. Lett.* **1993**, *214*, 215.

(37) Betts, T. A.; Zagrobelny, J.; Bright, F. V. *J. Am. Chem. Soc.* **1992**, *114*, 8163.

(38) Heitz, M. P.; Bright, F. V. *J. Phys. Chem.* **1996**, *100*, 6889.

(39) Anderton, R. M.; Kauffman, J. F. *J. Phys. Chem.* **1995**, *99*, 13759.

(40) A "repulsive" mixture is one in which a local density *depletion* is expected near the critical point. See for example: Debenedetti, P. G.; Mohamed, R. S. *J. Chem. Phys.* **1989**, *90*, 4528. Petsche, I. B.; Debenedetti, P. G. *J. Chem. Phys.* **1989**, *91*, 7075.

(41) For example, we have measured the rotation time of PRODAN in acetone to be ∼30 ps.

(42) Dote, J. L.; Kivelson, D.; Schwartz, R. N. *J. Phys. Chem.* **1981**, *85*, 2169.

(43) Ben Amotz, B. A.; Drake, J. *J. Phys. Chem.* **1988**, *88*, 1019.

(44) Bunker, C. E.; Sun, Y.-P. *J. Am. Chem. Soc.* **1995**, *117*, 10865.

(45) International Thermodynamic Tables of the Fluid State: Carbon Dioxide, 1976.

(46) Ely, J. F.; Haynes, W. M.; Bain, B. C. *J. Chem. Thermodyn.* **1989**, *21*, 879.

(47) Vesovic, V.; Wakeham, W. A.; Olchowy, G. A.; Sengers, J. V.; Watson, J. T. R.; Millat, J. *J. Phys. Chem. Ref. Data* **1990**, *19*, 763.

(48) The equation proposed by Vesovic et al. includes a term for enhancement of viscosity in the critical region. We have omitted this term in our calculations due to the complexity of solving the associated equations, but find that there is, at worst, only a few percent difference in calculated viscosities at the conditions used herein.

(49) Besserer, G. J.; Robinson, D. B. *J. Chem. Eng. Data* **1973**, *18*, 137.

(50) Fleming, G. R. *Chemical Applications of Ultrafast Spectroscopy*; Oxford: New York, 1986.

(51) Tao, T. *Biopolymers* **1969**, *8*, 609.

(52) Perrin, F. *Phys. Radium* **1934**, *5*, 497.

(53) Youngren, G. K.; Acrivos, A. *J. Chem. Phys.* **1975**, *63*, 3846. Hu, C.-M.; Zwanzig, R. *J. Chem. Phys.* **1974**, *60*, 4354.

(54) *AMPAC 5.0*; Semichem: 7128 Summit, Shawnee, KS 66216, 1994.

(55) Bondi, A. *J. Phys. Chem.* **1964**, *68*, 441. Edwards, J. T. *J. Chem. Ed.* **1970**, *47*, 261.

(56) Cross, A. J.; Fleming, G. R. *Biophys. J.* **1984**, *46*, 45.

(57) Least-squares minimization is performed using a modified Levenberg−Marquardt algorithm based on the "ZXSSQ" subroutine (IMSL, Inc., 1976).

(58) See Horng, M.-L.; Gardecki, J.; Maroncelli, M. *J. Phys. Chem.* **1997**, *101*, 1030.

(59) Whereas there is no discernible polarity-dependent Stokes shift in TPP or PEA, there is a small shift in the case of BTBP. For example, comparing the Stokes shifts of BTBP observed in 2-methylbutane and DMSO, one finds a difference of 200 cm^{-1}. Evidently there is some part of the spectral shift of this molecule that is sensitive to the nuclear polarizability of the solvent.

(60) However, at sufficiently low densities we do observe emission from the quartz windows of the supercritical cell. The spike at ∼18 700 cm^{-1} and the rising intensity beyond 25 000 cm^{-1} in Figure 6 result from such window emission.

(61) The form we employ for the *B* term is nonstandard. It results from assuming that this "solvent Stark effect" is proportional to the magnitude of the solvent-induced mean squared electric field within the solute "cavity". Previous treatments use various complicated derivations of the magnitude expected for such fluctuations. However, within the context of a linear response formalism, the squared fluctuations in the field should be simply proportional to the reaction field that would be present if the solute were dipolar. Thus, for the solvent dependence of this term we use the standard reaction field applicable a polarizable solute.

(62) Baur, M. E.; Nicol, M. *J. Chem. Phys.* **1966**, *44*, 3337. Nicol, M.; Swain, J.; Shum, Y.-Y.; Merin, R.; Chen, R. H. H. *J. Chem. Phys.* **1968**, *48*, 3587.

(63) Lampert, R. A.; Meech, S. R.; Metcalfe, J.; Phillips, D.; Schaap, A. P. *Chem. Phys. Lett.* **1983**, *94*, 137;

(64) Berlman, I. B. *Handbook of Fluorescence Spectra of Aromatic Molecules*, 2nd ed.; Academic Press: New York, 1971.

(65) See for example the discussion in: Hirayama, S.; Phillips, D. *J. Photochem.* **1980**, *12*, 139, and references therein.

(66) Neither the study by Sun and Bunker nor that of ref 63 accounted for the variation of ν_{fl} with solvent conditions as we have done here, but this factor has a negligible effect on the power observed, especially in the CO_2 set. The study by Bunker and Sun did not extend to as low a density as the present results, and this difference may partially account for the different n_D dependence observed. However, some of the difference may also result from the samples in ref 44 being more rigorously free of oxygen than ours. We note that at the highest and lowest CO_2 densities available for comparison, our lifetimes are roughly 8 and 13% smaller than those plotted in Figure 4 of ref 44, which might be caused by the presence of a trace amount of oxygen quenching, whose effect on the lifetime might be (slightly) density dependent.

(67) For a discussion on the effects of a cluster environment on radiative rates see: Shalev, E.; Ben-Horin, N.; Jortner, J. *J. Chem. Phys.* **1991**, *94*, 7757. Gersten, J.; Nitzan, A. *J. Chem. Phys.* **1991**, *95*, 686.

(68) Actually, for the asymmetric rotors studied here the stick predictions do not correspond to exact monoexponential behavior, but rather to biexponential $r(t)$. However, the time constants are in all cases similar enough so as to be indistinguishable from a monoexponential in experiment. In the case of slip boundary conditions, TPP, since it is modeled as a symmetric oblate top, is calculated to have a biexponential $r(t)$ with one time constant being zero (clearly an unphysical result).

(69) Goulay-Bize, A. M.; Dervil, E.; Vincent-Geisse, *J. Chem. Phys. Lett.* **1980**, *69*, 319. Canonica, S.; Schmid, A. A.; Wild, U. P. *Chem. Phys. Lett.* **1985**, *122*, 529. Lee, M.; Bain, A. J.; McCarthy, P. J.; Han, C. H.; Haseltine, J. N.; Smith, A. B., III; Hochstrasser, R. M. *J. Chem. Phys.* **1986**, *85*, 4341. Kim, S. K.; Fleming, G. R. *J. Phys. Chem.* **1988**, *92*, 2168. Bowman, R. M.; Eisenthal, K. B. *Chem. Phys. Lett.* **1989**, *155*, 99. Brocklehurst, B.; Young, R. N. *J. Phys. Chem.* **1995**, *99*, 40.

(70) Zwanzig, R.; Harrison, A. K. *J. Chem. Phys.* **1985**, *83*, 5861.

(71) See Figure 9 of ref 68 and the discussion surrounding it.

(72) See, for example, the recent compilation and analysis in: Williams, A. M.; Jiang, Y.; Ben-Amotz, D. *Chem. Phys.* **1994**, *180*, 119.

(73) Although the dipole moment of CO_2 is zero, CO_2, like benzene, possesses a large quadrupole moment that renders it significantly "polar" in that a sizable part of its interactions with dipolar or other quadrupolar molecules results from Coulombic interactions between the permanent charge distributions of the two species. Solvatochromic studies [Reynolds, L.; Gardecki, J. A.; Frankland, S. J. V.; Horng, M.-L.; Maroncelli, M. *J. Phys. Chem.* **1996**, *100*, 10337] place the polarity of CO2 at high density ($\rho_r \approx 2$) near that of a dipolar liquid with $\epsilon_0 \approx 5$.

(74) Horng, M.-L.; Maroncelli, M. Unpublished results.

(75) In the case of rotation times and spectral shifts, this relationship is indirect. The $F(\rho)$ functions here entail intermediate connections to the solvent viscosity or refractive index, the latter which can be expressed as simple functions of solvent density.

(76) In employing eq 12 we have neglected possible variations of the *B* term in eq 6 with solvent density. This last term arises from interactions between the solute and the permanent charge moments of the solvent. It is hard to include this effect since the static dielectric constant of CO_2 does not represent such interactions. However, we have tested the likely effect of omitting this term by making the assumption that at the highest density CO_2 has an effective dielectric constant of ∼5 [ref 73] and that the factor $(\epsilon_0 - 1)/(\epsilon_0 + 2)$ is simply proportional to density. Due to the small size of the *B* coefficient deduced from the liquid studies, we find that this omission has an effect on the results that is well within the anticipated uncertainties of the determination of ρ_{eff}.

(77) In the case of DPB there is sufficient liquid phase data, mainly in alcohol solvents, [Anderton, R. M.; Kauffman, J. F. *J. Phys. Chem.* **1994**, *98*, 12117] with which to roughly assess the "normal" hydrodynamic behavior of this solute. A plot of these liquid solvent data along side the CO_2 results from ref 39 in the form of a plot of C_{obs} versus viscosity looks similar to the bottom panel of Figure 11 (PEA data). In particular, there is a strong dependence of C_{obs} on CO_2 density that we would interpret as reflecting local density augmentation, with maximal $(\Delta\rho/\rho)$ of ∼100% occurring at the lowest density studied, $\rho_r \approx 0.8$. In the case of the HMS solute, C_{obs} does not appear to vary with CO_2 density. One might therefore conclude that augmentation has a negligible effect on rotational motion of this solute. However, we note that the values of C_{obs} are higher in supercritical CO_2 (∼1) than in the two liquids studied (hexane C_{obs} ∼0.6, ethanol C_{obs} ∼0.4). On this basis it could be argued that there is a density-independent local density augmentation in CO_2 that gives rise to this difference. The latter is in essence what Anderton and Kauffman propose.[39] We would favor the former interpretation. In any case, the differences between the conclusions reached in ref 39 and in our analysis of the same data illustrate the difficulty of attempting to quantifying local density augmentation. A thorough understanding of the behavior in the absence of augmentation must be available either from empirical or theoretical considerations in order to accurately determine the magnitude of the deviations that provide augmentation estimates. In many cases our understanding is only partial so as to provide a wide margin of expected behaviors, which in turn lead to large uncertainties in local density estimates.

(78) Heitz, M.; Maroncelli, M. Unpublished results.

(79) See for example: Stanley, H. E. *Introduction to Phase Transitions and Critical Phenomena*; Oxford Press: New York, 1971.

(80) These two methods are reviewed in the two articles by J. R. Lakowicz and I. Gryczynski and D. J. S. Birch and R. E. Imhof in the book: *Topics in Fluorescence Spectroscopy, Vol. 1: Techniques*; Lakowicz, J. R., Ed.; Plenum: New York, 1991.

(81) Lakowicz, J. R.; Jayaweera, R.; Joshi, N.; Gryczynski, I. *Anal. Biochem.* **1987**, *160*, 471.

(82) Maroncelli, M. Unpublished results.

(83) Collaborative work planned with Frank Bright.

(84) See, for example the lucid discussion in: Randolph, T. W.; O-Brien, J. A.; Ganapathy, S. *J. Phys. Chem.* **1994**, *98*, 4173.